Impact Experiments into Borosilicate Glass at Three Scale Sizes

Charles E. Anderson, Jr.

Carl E. Weiss

Sidney Chocron

Southwest Research Institute®
P.O. Drawer 28510
San Antonio, TX 78238

Contract: W56HZV-06-C-0194

SwRI® Report 18.12544/018

Prepared for:

US Army RDECOM-TARDEC
AMSRD-TAR-R
Warren, MI 43897-5000

November 2009

REPORT DOCUMENTATION PAGE

Form Approved
OMB No. 0704-0188

1. REPORT DATE *(DD-MM-YYYY)*	2. REPORT TYPE	3. DATES COVERED *(From - To)*
30-11-2009	Technical	May 2008 – Nov. 2009

4. TITLE AND SUBTITLE

Impact Experiments into Borosilicate Glass at Three Scale Sizes

5a. CONTRACT NUMBER
W56HZV-06-C-0194

5b. GRANT NUMBER

5c. PROGRAM ELEMENT NUMBER

6. AUTHOR(S)

Charles E. Anderson, Jr., Carl E. Weiss, and Sidney Chocron

5d. PROJECT NUMBER
18.12544

5e. TASK NUMBER

5f. WORK UNIT NUMBER

7. PERFORMING ORGANIZATION NAME(S) AND ADDRESS(ES)

Southwest Research Institute
P.O. Drawer 28510
San Antonio, TX 78238-0510

8. PERFORMING ORGANIZATION REPORT NUMBER
18.12544/018

9. SPONSORING/MONITORING AGENCY NAME(S) AND ADDRESS(ES)

US Army Tank-Automotive Research, Development, and Engineering Center
Warren, MI 48397-5000

10. SPONSOR/MONITOR'S ACRONYM(S)
RDECOM-TARDEC

11. SPONSORING/MONITORING AGENCY REPORT NUMBER

12. DISTRIBUTION AVAILABILITY STATEMENT

Approved for Public Release; Unlimited Distribution

13. SUPPLEMENTARY NOTES

The views, opinion, and/or findings contained in this report are those of the authors and should not be construed as an official Department of the Army position, policy, or decision, unless so designated by other documents.

14. ABSTRACT

Glass impact experiments were designed at three different scales—0.22-cal, 0.375-cal, and 0.50-cal—named after the diameter of the bullets. Four experimental series were conducted at the three scale sizes: 1) Lexan-only experiments; 2) monoblock glass experiments; 3) single impact bonded glass experiments, and 4) multi-hit experiments. The experiments were conducted to obtain residual velocity as a function of impact (striking) velocity, including sufficient partial penetrations to calculate a V_{50}. The $V_s - V_r$ data were fit to the Lambert equation, Eqn. (5), to obtain another estimate of V_{50}. Eroded lengths of the bullets were also measured. The objective of the experiments was to investigate whether a time dependency exists in glass damage/failure for ballistic experiments, and if so, try to quantify this dependency. No scale effect was observed in experimental results for the Lexan-only experiments. But a variety of scale effects were observed in the glass impact experiments, suggesting that there exists a time dependency to failure that is important within the timeframe of ballistic events.

15. SUBJECT TERMS

borosilicate glass, residual velocity, V50, scaling, time-dependent fracture, small arms, monolithic bullets, Lexan, polycarbonate, damage, dwell

16. SECURITY CLASSIFICATION OF:			17. LIMITATION OF ABSTRACT	18. NUMBER OF PAGES	19a. NAME OF RESPONSIBLE PERSON
					Dr. Douglas Templeton
a. REPORT	b. ABSTRACT	c. THIS PAGE	None	76	19b. TELEPONE NUMBER (*Include area code*)
Unclassified	Unclassified	Unclassified			586-574-5325

Table of Contents

Page

List of Figures

Page

List of Figures (Cont'd)

Page

List of Figures (Cont'd)

Page

List of Tables

Page

1.0 Introduction

There has been considerable discussion in the technical community concerning the existence of so-called failure waves in glass, Refs. [1-5] and reference citations in these articles. Recent work at Southwest Research Institute (SwRI) has focused on the penetration performance of gold rods into lead and borosilicate glass [6-8]. Some of the testing has concentrated on the conditions for dwell and interface defeat [9-10]. A distinction between the work at SwRI and most others is the stress state in the glass as damage nucleates and propagates [5]. Flyer plate impact is uniaxial strain; bar-on-bar impact is an uniaxial stress condition, and Taylor impact is somewhere in between. Edge-on impact, such as done by researchers at the Ernst-Mach-Institut [11-12] provides a complicated stress state that is dominated by the presence of free surfaces. However, a penetrating rod (or projectile) has a divergent, hemispherical-like stress field.

Grady [13] has suggested that failure of glass is time dependent. An important question that needs to be addressed is whether the time dependency is important for ballistic impacts of interest. For example, the Tuler-Butcher model [14] is a time-dependent failure model that has been applied to metal spallation:

$$D = \int_0^t (\sigma - \sigma_o)^\beta \, dt \tag{1}$$

where D represents damage (it goes from 0 for no damage, to 1.0 for fully damaged). Damage accumulates with time, t, and applied overstress. There is a stress threshold, σ_o below which no damage accumulates. The parameter β is a material parameter, which often has a value of 2, but can be adjusted to provide better agreement between simulations and experiment.

The time derivative of Eqn (1) gives:

$$\dot{D} = (\sigma - \sigma_o)^\beta \tag{2}$$

so it is readily seen that the damage rate depends upon the overstress. Typically, if the applied overstress is very large, damage very quickly saturates, the time dependency is not particularly important, and failure can be replaced by a sudden-damage parameter, e.g., a strain-to-failure or a stress-to-failure condition.

It is not known if the time scale of failure might be important for glass, as suggested by Grady [13]. Therefore, we designed a series of experiments to investigate if time dependency could be observed in ballistic impact. The objective was to quantify any time dependency, if it existed, and help to assess whether it was sufficiently large that a glass constitutive model would be required to account for this time dependency. Additionally, the set of experiments could provide useful experimental data for model validation.

The next section describes the scaling laws applicable to the experiments. Sections 3 and 4 provide details of target design and construction, and define the projectiles that were used in the experiments. The experimental results are given in Section 5, and conclusions of the technical effort are summarized in Section 6.

2.0 Scaling Laws

A detailed similitude analysis was conducted by Anderson, *et al*. [15-16], for replica scaling of ballistic experiments. Here, we only summarize some of the salient features germane to these glass impact experiments.

Letting the symbol λ represent the scale factor, then the model law for replica modeling is summarized in Table 1. The model law states that all the geometric lengths are scaled by the factor λ, but the material strength and density are the same as for full scale, i.e., $\lambda = 1.0$. Thus, as implied by the term "replica model," the same material is used in the model as in the prototype (full scale). However, the mass (because each geometric dimension is scaled by λ) is reduced by λ^3. The impact conditions remain the same for the replica model (i.e., the same impact velocity), which results in the same pressures and stresses in the target for the model as the prototype. However, there is a contradiction on the strength. Strain rates are higher in the model target by a factor of λ^{-1}. Many materials have a strength that is strain rate dependent; thus, for example, since the strain rate is larger in the model target, then the model displays a higher strength than the prototype target. However, strain rate effects typically are logarithmic, and it takes very large changes in scale size for strain rate effects to result in a significant change in strength between model and prototype.[1]

Table 1. Replica Model Law

Parameter	Scale Factor
Geometric lengths	λ
Velocity	1.0
Strength	1.0
Density	1.0
Mass	λ^3
Pressure	1.0
Stress	1.0
Strain rate	λ^{-1}
Time	λ
Surface flaws	λ^2
Volume flaws	λ^3
Fracture toughness	$\lambda^{1/2}$

Size effects are often discussed in relation to the strength of brittle materials (typically, the strength in tension). The usual argument is that failure is initiated at some geometric or material flaw. The probability of encountering a flaw larger than some size typically follows some probability distribution function, such as a Weibull distribution. The larger the specimen, the higher the probability of encountering a flaw that exceeds a critical flaw size; i.e., smaller

[1] It was shown in Ref. [15] that changes in a scale factor of 10 resulted in 5% or less difference in residual velocity and residual length of a projectile perforating a finite-thick steel target. For the cases examined here, the maximum change in scale factor is 2.27, which implies that the maximum differences in penetration response would be on the order of 1%, which is considerably less than typical experimental scatter/uncertainties.

specimens appear stronger than larger specimens. Wereszczak, *et al.* [17], conducted indentation and biaxial flexure experiments and showed that the characteristic tensile failure stress increased by approximately a factor of two with a two orders of magnitude decrease in the effective area. For the experiments reported here, the maximum change in area is approximately 5, which would correspond to a 30% increase in the characteristic tensile failure stress as the specimen size is decreased. However, it has also been shown that variability in strength decreases considerably under confinement [18], and in the ballistic event, compressive and shear stresses dominate during penetration. Therefore, although not definitive, we do not think that distributions of surface and volume flaws are responsible for differences that might be seen in the ballistic response at the differences in scale sizes under investigation.

Of particular relevance here is that time scales as the scale factor; that is, it takes less time to perforate the scaled target, all other things being equal. However, damage accumulation depends upon absolute time, as indicated in Eqn. (1). Curran, *et al*. [19], describe nucleation and growth of damage from a microscopic viewpoint, and explicitly describe the nucleation and growth as functions of time. In the micromechanical model, similar to the Tuler-Butcher model, the amount of overstress drives damage accumulation. Thus, only near a threshold condition where the overstress is not large—such as a ballistic limit—would it be expected that any time dependency might be noticeable. The scaled target would appear to be "stronger" because there was less time for the damage to develop. This was exactly what was observed in ballistic limit experiments at three scales in Ref. [16].

It is this last observation that motivated the experiments. It was decided to conduct ballistic impact experiments at three different scales. For the experiments to be directly relevant to transparent armor, the threats were small caliber (between 0.22 cal and 0.50 cal). The next section describes application of the replica model scaling laws to design the three target sets.

3.0 Experimental Design

3.1 Glass Targets

The glass selected for the experimental study was a borosilicate glass, Borofloat® 33, manufactured by Schott North America. The material properties of Borofloat 33 are given in Table 2. This glass was selected because of complementary studies using the same glass [6-8,18,20].

It was decided to fabricate two target types: 1) a monoblock glass target, and 2) a monoblock glass target at the same thickness as item 1, but backed by a polycarbonate layer. Real transparent armors are a series of glass layers bonded with different types of adhesives. Almost all transparent armors have a polycarbonate layer as the final layer (to suppress spall), and most transparent armors have polycarbonate inner layers. However, the focus of this study was to investigate the penetration performance of glass and determine if there might be a time-dependent effect in the failure dynamics of glass. Thus, we wanted to keep the experiments as simple as possible, without the complication of adhesive and other inner layers. Nevertheless, one of the target sets did have a polycarbonate back layer (substrate) because of concerns of about the failure dynamics of the monoblock glass target (as will be discussed later).

Table 2. Material Properties for Borosilicate Glass (Borofloat® 33)

Density [g/cm^3]	Young's modulus [GPa]	Knoop hardness [kp/mm^2]	Poisson's Ratio	Longitudinal wave speed [km/s]	Transverse wave speed [km/s]	HEL [20] [GPa]
2.2	62.3	480	0.2	5.61	3.41	8.7

Targets were designed at three scales, nominally to different threat calibers, e.g., 0.50-cal, 0.30-cal, and 0.22-cal. The 0.50-cal projectile is considered to be the prototype, i.e., full-scale, target, with $\lambda = 1.0$. It was realized that these three scales probably could not be maintained exactly because of constraints on purchasing target elements at the appropriate thicknesses. Thus, instead of using conventional bullets, which also might not adhere to the scaling laws, it was decided to use monolithic bullets that were essentially modified fragment simulating projectiles (FSPs). The projectiles will be described after a discussion of target design.

3.2 Initial Geometric Design of Glass Targets

The initial target design assumed that glass was procured using off-the-shelf glass thicknesses. Projectile dimensions would be adjusted to maintain scaling; likewise, polycarbonate (Lexan®) dimensions would be adjusted to maintain scaling. The thicknesses available for Borofloat® 33 are shown in Table 3. Thicknesses are given in millimeters (inches) with tolerances.

Given these off-the-shelf thicknesses, three glass thicknesses were selected to be as close as possible to scaling of 0.50-, 0.30-, and 0.22-caliber projectiles. It was also decided to make the thickness of the polycarbonate substrate layer equal to the diameter of the projectile. The three initial target designs (two target types per threat bullet) are shown in Fig. 1. A mixture of metric and English units is used since bullet caliber is measured in inches. The scale size listed in the figure captions are "nominal" scale sizes. The actual scale size is dictated by the projectile diameter.

Table 3. Thickness Availability of Borofloat 33 (from Schott North America)

Thickness		Tolerance	
0.70	(0.027)	± 0.07	(0.003)
1.10	(0.043)	± 0.1	(0.004)
1.75	(0.069)	± 0.2	(0.008)
2.00	(0.079)	± 0.2	(0.008)
2.25	(0.089)	± 0.2	(0.008)
2.75	(0.108)	± 0.2	(0.008)
3.30	(0.130)	± 0.2	(0.008)
3.80	(0.150)	± 0.2	(0.008)
5.00	(0.197)	± 0.2	(0.008)
5.50	(0.216)	± 0.2	(0.008)
6.50	(0.256)	± 0.2	(0.008)
7.50	(0.295)	± 0.3	(0.012)
8.00	(0.315)	± 0.3	(0.012)
9.00	(0.354)	± 0.3	(0.012)
11.00	(0.433)	± 0.3	(0.012)
13.00	(0.512)	± 0.3	(0.012)
15.00	(0.590)	± 0.3	(0.012)
16.00	(0.630)	± 0.5	(0.020)
17.00	(0.670)	± 0.5	(0.020)
18.00	(0.708)	± 0.5	(0.020)
19.00	(0.748)	± 0.5	(0.020)
20.00	(0.787)	± 0.7	(0.027)
21.00	(0.827)	± 0.7	(0.027)

Thicknesses are given in mm (inches) with tolerances

3.3 Final Glass Target Design

Schott North America was contacted about target fabrication, particularly fabrication of the glass/Lexan targets. Their recommendation was not to mill the polycarbonate since milling could affect transparency and potentially affect material properties. Schott North America stated that grinding the glass to desired dimensions was not a problem. Therefore, the targets were redesigned based on thickness availability of Lexan (the polycarbonate). Lexan 9034 is a high-impact polycarbonate without a coating, and was the polycarbonate recommended by Schott North America. Lexan 9034 comes in the following thicknesses: 12.70 mm (0.50 inch), 9.52 mm (0.375 inch), and 5.59 mm (0.22 inch).[2]

Given the thickness availability of Lexan, combined with the constraint that the Lexan not be machined, but used "as delivered," a new target design was developed. The three final target designs are shown in Fig. 2.

The lateral dimensions of the targets, which were also scaled, were: 46.2 cm x 46.2 cm (0.50 cal); 34.6 cm x 34.6 cm (0.375 cal); and 20.3 cm x 20.3 cm (0.22 cal).

[2] It is clear, simply by looking at the dimensions, that Lexan is manufactured using English units.

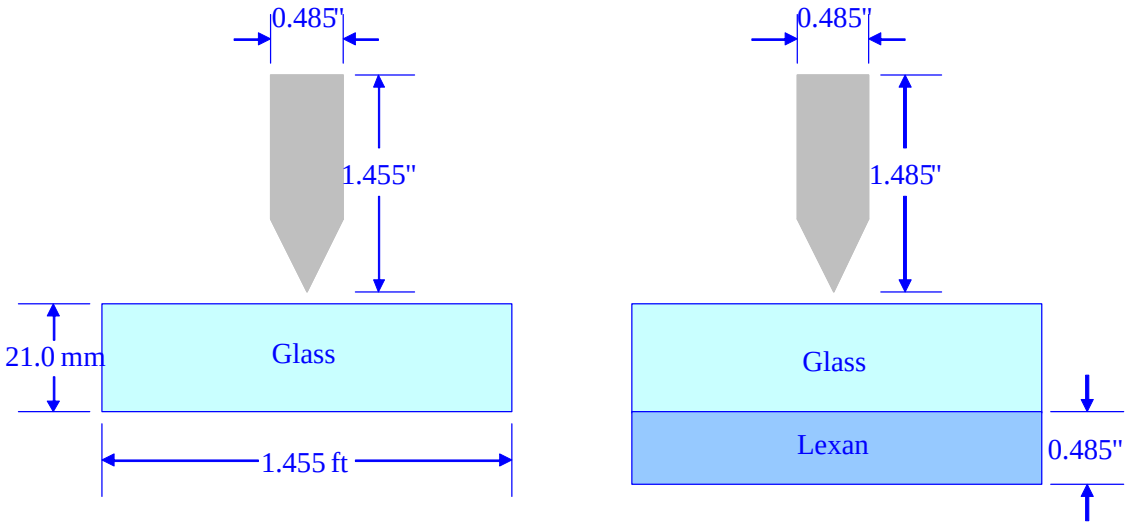

(a) Nominal 0.50-cal target design.

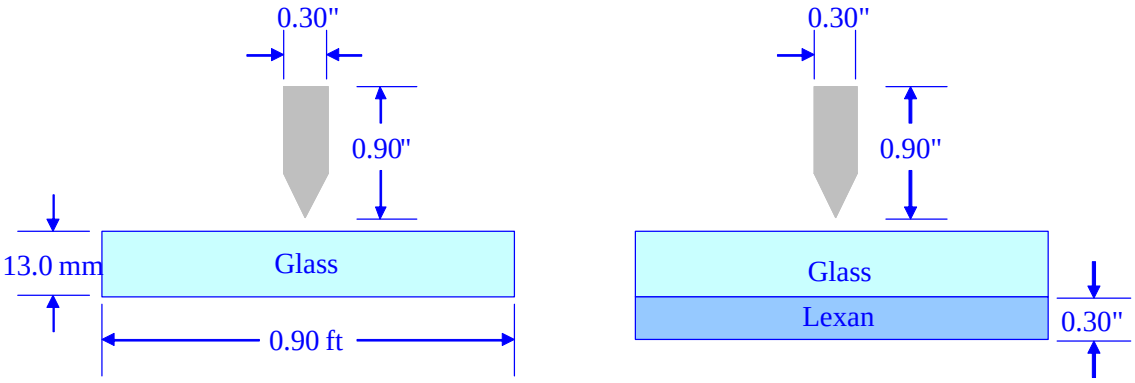

(b) 0.30-cal target design.

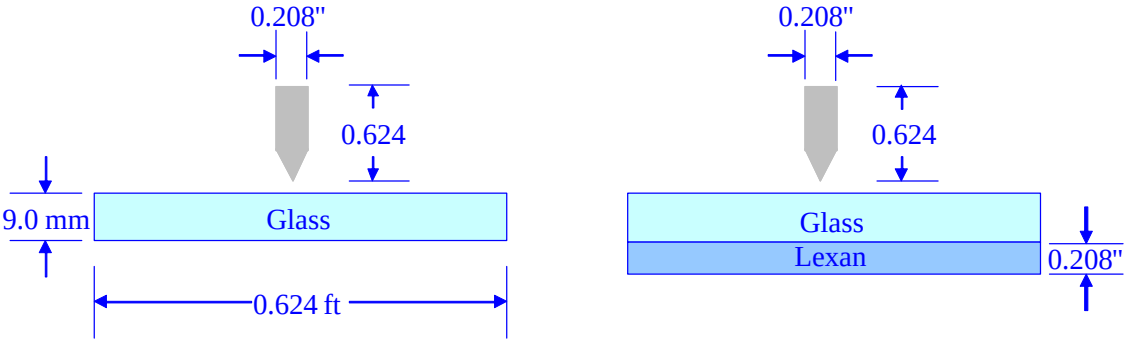

(c) Nominal 0.22-cal target design.

Figure 1. Initial target designs, based on off-the-shelf thicknesses of glass (thicknesses and bullets are to scale, but not lateral plate dimensions).

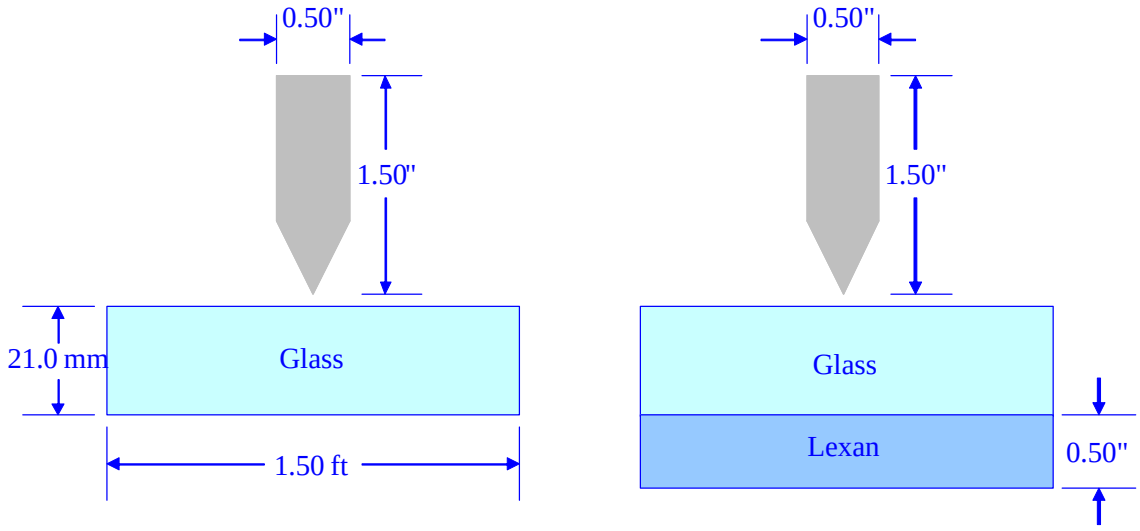

(a) 0.50-cal target design.

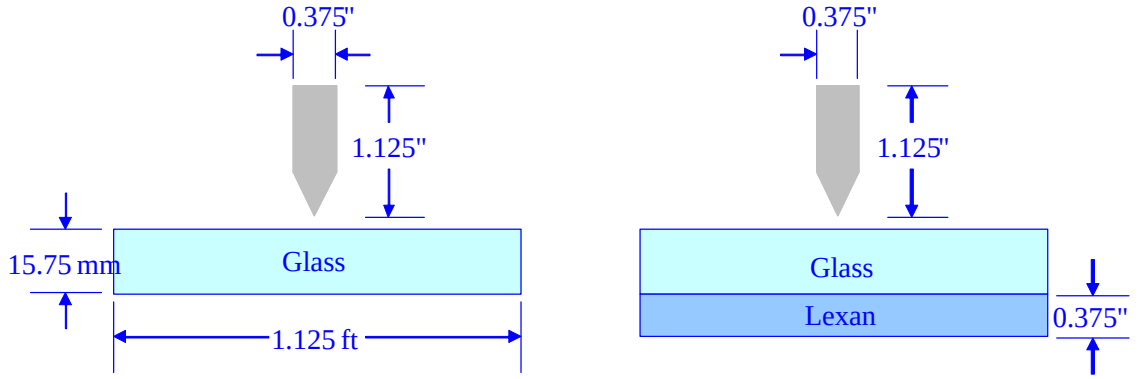

(b) 0.375-cal target design.

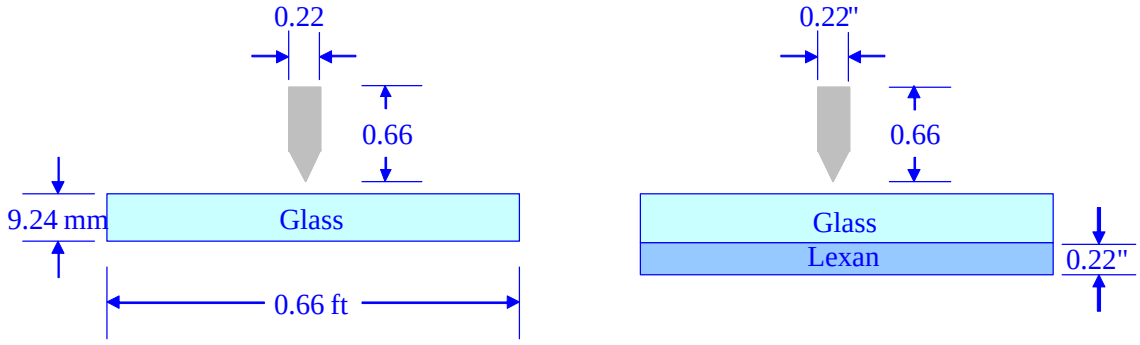

(c) 0.22-cal target design.

Figure 2. Final target designs, based on off-the-shelf thicknesses of Lexan (thicknesses and bullets are to scale, but not lateral plate dimensions).

3.4 Target Fabrication/Assembly

The glass pieces were ground and polished to the desired dimensions by Schott North America. Grinding changes the surface quality and also brings internal striation closer to one surface than the other. Therefore, Schott North America removed the tin side by grinding (tolerance 0.01 mm or better). The polished side was bonded (when applicable) to the Lexan substrate.

The adhesive used between the glass and polycarbonate must compensate for the mismatch of thermal expansion between glass and Lexan, without degrading the Lexan. Liquid adhesives embrittle, and hence degrade, polycarbonate performance. According to Schott North America, the choice of the interlayer will affect the outcome of a test, and that it is better to use a hard interlayer versus a soft one. Their suggestion was to use Huntsman PE399 polyurethane. Given Schott North America's experience in fabricating and manufacturing transparent armor, we elected to follow their advice.

Huntsman PE399 polyurethane comes in the following thicknesses: 75 mils, 50 mils, 25 mils, and 22 mils. Lamination of films requires an autoclave, and the laminator should have experience with laminating polycarbonate with glass. Additionally, polyurethane is sensitive to humidity; thus, the dryer the environment in which the film is processed, the better the results. Therefore, it was decided to let Schott North America fabricate the glass/polycarbonate targets.

The adhesive thicknesses do not scale exactly with the three scale sizes selected, but they are approximate:

- 75 mils adhesive → 12.7 mm (0.500 in) Lexan
- 50 mils adhesive → 9.52 mm (0.375 in) Lexan (should be 56.2 mils of adhesive)
- 25 mils adhesive → 5.59 mm (0.220 in) Lexan (should be 33 mils of adhesive)

The thicknesses at the end of the last two bulleted items denote the thickness of the adhesive layer for perfect scaling. It was determined that we should not modify the thickness of an adhesive layer since it could affect bonding properties. In fact, Schott North America was somewhat concerned with the 25-mil thickness (they had no experience with this thickness). They fabricated a specimen and conducted a pull test, determining that the adhesive worked quite well.

3.5 Projectile Design and Heat Treat

Projectiles were designed to shoot from a rifled barrel to achieve spin stabilization. Thus, an FSP-like design was adopted for engaging the rifling.[3] The projectiles were designed with a 52° conical nose (the nose length was one-third the total length). The shanks of the projectiles were slightly undersized from the skirts that engaged the barrel rifling grooves. Machine drawings for the projectiles are shown in Fig. 3. A photograph of the fabricated projectiles is shown in Fig. 4.

The projectiles were fabricated from 4340 steel (similar to an FSP). Initially, the 4340 steel was heat treated to a Rockwell C (Rc) hardness of 30; similar to the requirement for FSPs. The objective was for the bullets to penetrate in a rigid-body model into the glass to eliminate

[3] A special 0.375-caliber barrel had to be ordered to shoot the 0.375-cal bullet.

projectile deformation.[4] In some preliminary "scoping" experiments, it was observed that there was considerable mushrooming of the bullet nose, as shown in Fig. 5. Therefore, the bullets were returned for an additional heat treat, hardening the steel to Rc53.

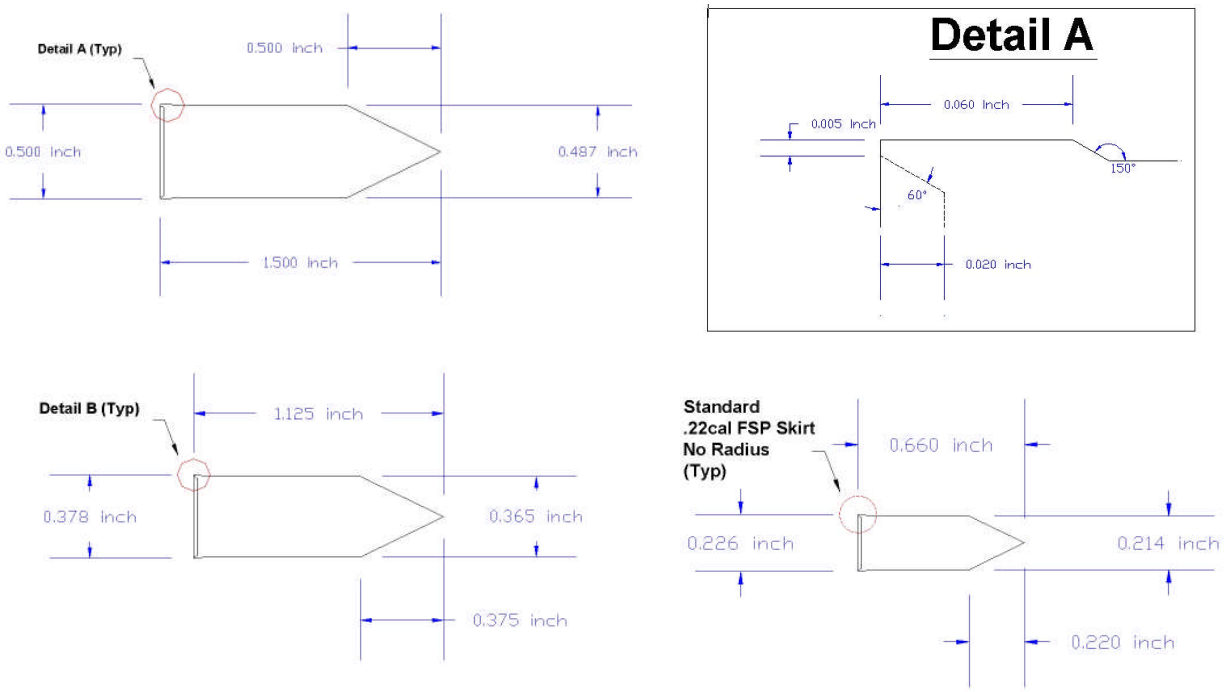

Figure 3. Machine drawings for projectiles (upper left: 0.50 cal; lower left, 0.375 cal; lower right, 0.22 cal. The upper right drawing (Detail A) provides details on the skirt that engages the rifling.

Figure 4. Photograph of the three projectiles.

Figure 5. Photograph of 0.50-cal bullet (Rc30) showing considerable nose erosion and mushrooming.

[4] One of the objectives of the experiments was to provide fundamental ballistic response data for validation of a computational glass model. Elimination of bullet deformation removes this variable for model comparisons.

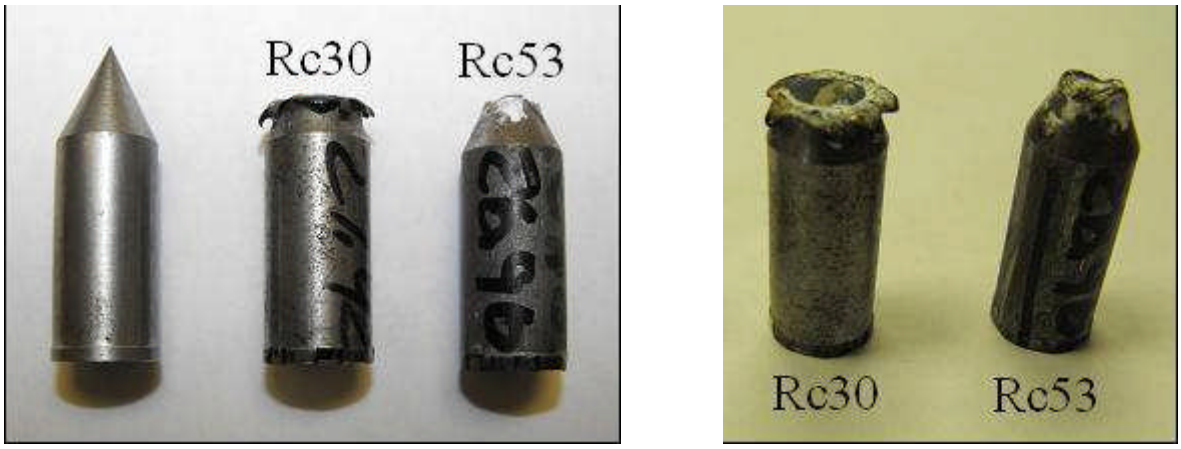

(a) Side view of damage to bullets. **(b) Top view of damaged bullets.**

Figure 6. Photographs of damaged bullets with different heat treatments.

As can be seen in Fig. 6, the hardened bullet under certain impact conditions—to be described later—still eroded. However, because the bullet material was now considerably more brittle, virtually no mushrooming of the bullet occurred. It was felt that this condition would be easier to model than combined mushrooming and erosion.

3.6 Summary

Three scale sizes were selected for the targets. Scale sizes were initially selected on the basis of availability of glass thickness, but this was changed to availability of thicknesses for the polycarbonate substrate. The glass was ground and polished to the correct thickness. Special purpose projectiles were designed at the three scale sizes: 0.50 caliber, 0.375 caliber, and 0.22 caliber.

4.0 Project Material Characterization

4.1 Introduction

Johnson-Cook strength and damage parameters exist for 4340 steel, Rc30 [21]; however, they do not exist for the Rc53 material. A limited set of characterization experiments were conducted so as to provide appropriate Johnson-Cook constants for the Rc53 material. The following tests were performed:

- Quasi-static and 1 s^{-1} tensile tests using smooth tensile samples. These tests were used to define the constants *A*, *B* and *n* in the Johnson-Cook plasticity model.
- Split-Hopkinson bar compression at a strain rate of ~1600 s^{-1}. These tests allowed the determination of the strain rate constant *C* in the Johnson-Cook plasticity model.
- Quasi-static compression tests to estimate a strain to failure in compression.

Since many tests are missing from this characterization (e.g., torsion, high temperature, notched samples, etc.) the constitutive models proposed below assume that some of the constants determined for the Rc30 material are applicable.

4.2 Johnson-Cook Strength Model

The quasi-static, medium rate (1 s^{-1}), and dynamic (~1600 s^{-1}) test results are plotted together in Fig. 7. Also shown in the same graph, with black lines, are the Johnson-Cook fits obtained for the different strain rates. The material does not seem to exhibit strengthening at low strain rates of ~1 s^{-1} but does show strengthening at Hopkinson bar rates. In order to capture the strengthening at large strain rates, the model must show some effect at moderate strain rates (because of the form of the model).

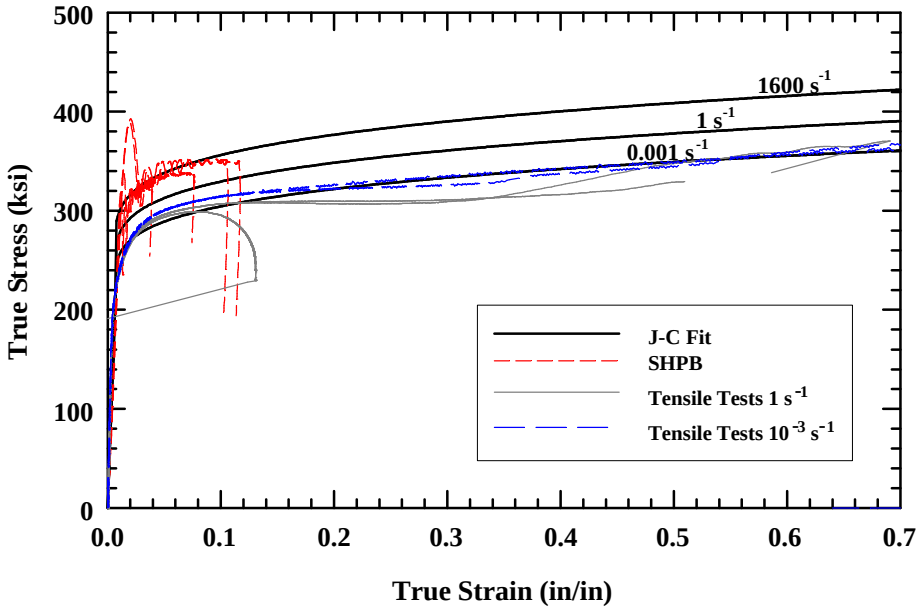

Figure 7. Characterization test results and Johnson-Cook fits to data.

The Johnson-Cook strength model [22] is used to compute the equivalent stress, σ_{eq}, as a function of strain, strain rate, and temperature, and has the form:

$$\sigma_{eq} = \left[A + B\varepsilon_p^{\,n}\right]\left[1 + C\ln\left(\dot{\varepsilon}/\dot{\varepsilon}_0\right)\right]\left[1 - T^{*m}\right]$$
$$T^* = \frac{T - T_{room}}{T_{melt} - T_{room}} \qquad (3)$$

where ε_p is the plastic strain, $\dot{\varepsilon}$ is the strain rate, $\dot{\varepsilon}_0$ is a reference strain rate of 1 s^{-1}, and T^* is the homologous temperature. The material constants are *A, B, C, n* and *m*. The constants estimated from the characterization experiments described above are listed in Table 4. No high temperature tests were used, so *m* from tests done with Rc30 4340 steel was used. It was also assumed that the melt temperature was the same as for Rc30 4340 steel.

Table 4. Johnson-Cook Strength and Damage Constitutive Constants for Rc53 4340 Steel

Strength		Damage	
A	1.55 GPa	D_1	-1.0
B	1.24 GPa	D_2	2.1
n	0.23	D_3	-0.5
C	0.011	D_4	0.002
m	1.03	D_5	0.61
T_{melt}	1520°C	σ_{spall}	6.76 GPa
T_{room}	25°C	ε^f_{min}	0.040

The stress-strain response of the Rc53 steel is compared to the Rc30 steel in Fig. 8. The heat treatment has approximately doubled the strength of the steel, but as will be shown, at the expense of ductility.

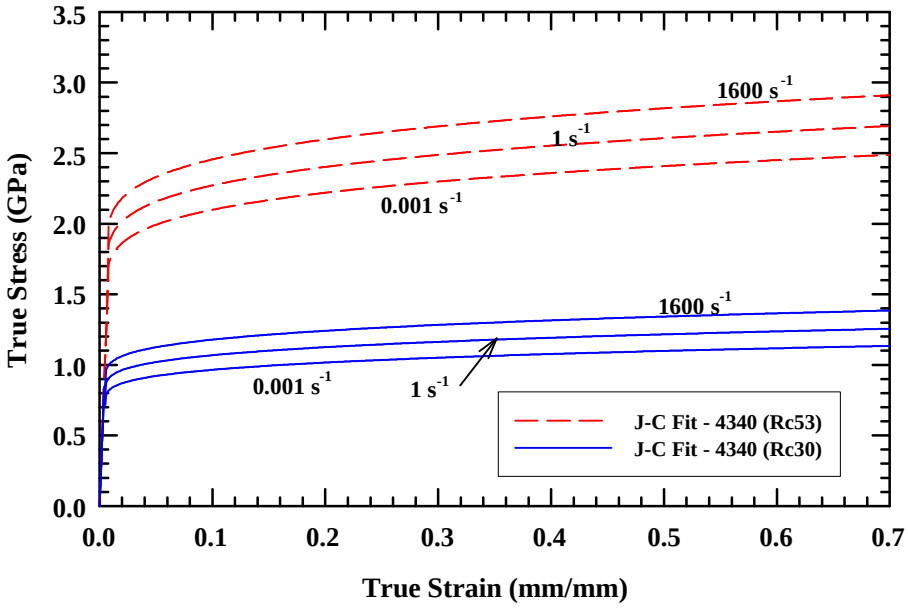

Figure 8. Comparison of hardened (Rc53) 4340 steel with literature data (Rc30) 4340 steel.

The adiabatic stress-strain curves for the two different heat treatments, at a strain rate of 10^3 s^{-1}, are shown in Fig. 9. For these adiabatic stress-strain curves, 100% of the plastic work is assumed to be converted into internal energy, thereby increasing the temperature of the material. The thermal term in the Johnson-Cook strength model then results in a softening of the material as plastic work accumulates.

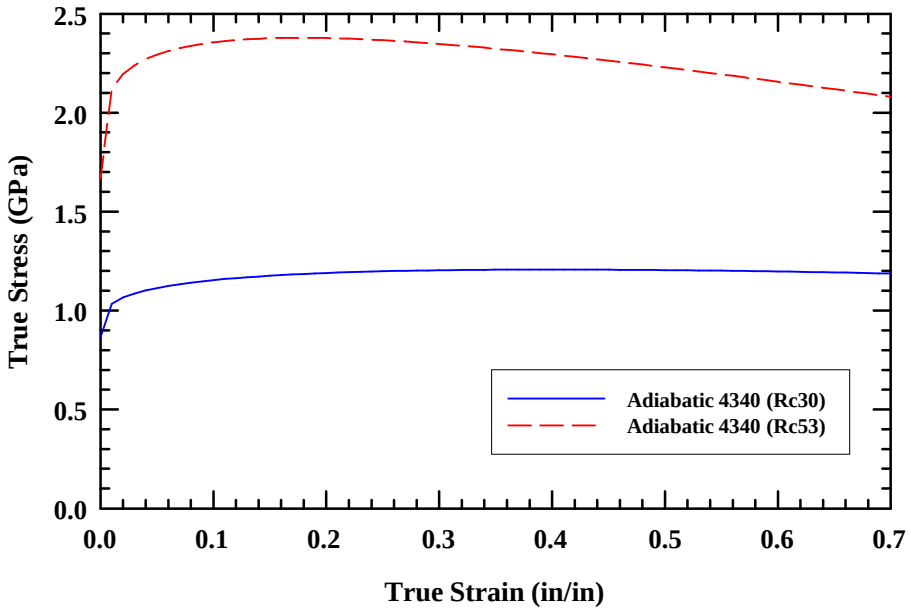

Figure 9. Adiabatic stress-strain curves for Rc30 and Rc53 4340 steel.

4.3 Johnson-Cook Damage Model

Very limited test data were available to determine the failure model as only smooth tension and compression tests were performed with the hardened Rc53 material. The Johnson-Cook damage model has the following form [23]:

$$\varepsilon_f = \left[D_1 + D_2 \ e^{D_3 \sigma^*} \right] \left[1 + D_4 \ln \left(\dot{\varepsilon} / \dot{\varepsilon}_0 \right) \right] \left[1 + D_5 T^* \right] \tag{4}$$

where σ^* is the triaxiality (or pressure-stress ratio, i.e., the mean stress divided by the equivalent stress), and D_1 through D_5 are the damage constants, and the strain rate and homologous temperature have the same definitions as used in Eqn. (3). The strain to failure data, as a function of the pressure-stress ratio, are shown in Fig. 10. The pressure-stress ratio was estimated through numerical simulations with LS-DYNA. The curve fit to the data was performed by translating the curve provided by Johnson and Holmquist [21]. The damage constants are summarized in Table 4.

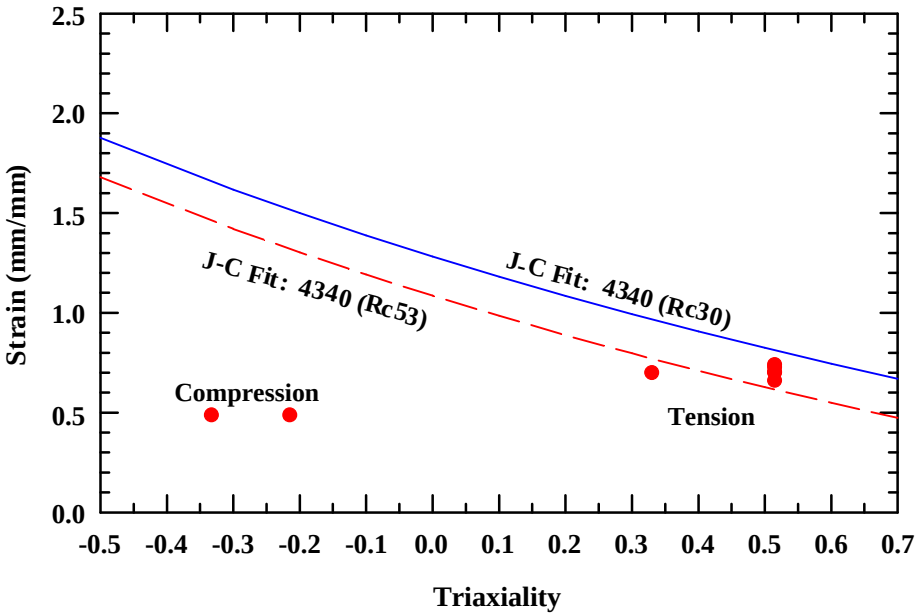

Figure 10. Johnson-Cook failure data and fit to model.

5.0 Experimental Results

5.1 Experimental Procedures

There were four sets of experiments for each bullet caliber:

- Lexan® only,
- Monoblock glass, one shot per target,
- Glass bonded to Lexan substrate, one shot per target, and
- Glass bonded to Lexan substrate, 5 shots per target.

The impact (striking) velocity (V_s) and residual velocity (V_r) were measured for each experiment. V_{50} was estimated from this information. V_{50} was determined by two methods: the traditional averaging of complete (CP) and partial (PP) penetrations, and by a regression fit to Lambert's equation [24]:[5]

$$\begin{aligned} V_r &= 0 & V_s &\le V_{\mathrm{BL}} \\ V_r &= a\left(V_s^{\,p} - V_{\mathrm{BL}}^{\,p}\right)^{1/p} & V_s &> V_{\mathrm{BL}} \end{aligned} \tag{5}$$

where a, p, and V_{BL} are regression fit parameters. Occasionally, near a ballistic limit, a perforating projectile will exit the target at a large angle and not be recorded in the high-speed camera images. For these experiments, there is no residual velocity, but we know that the impact velocity was only slightly above the ballistic limit velocity.

The overall experimental layout is shown in the photograph in Fig. 11. All projectiles were fired using rifled barrels mounted in a universal receiver. A bore mounted laser was used to confirm the impact location and target obliquity. For safety reasons the gun was fired remotely using a lanyard.

Projectile impact velocity was measured using Oehler Model 57 photoelectric chronographs located between the gun mount and the target fixture. The spacing between each chronograph was 45.7 cm. A calibrated Hewlett Packard HP 53131A universal counter, triggered by the chronographs, recorded the time it took the projectile to travel between chronograph screens. Projectile velocity was then calculated using the recorded times and known travel distance. (The distance between the gun and the center of the chronograph set was 1.5 m. The target holder was 3.0 m from the gun.)

An IMACON 200 ultra high-speed camera was used to image the strike face of the samples very near the point of impact. The camera was run at 100,000 frames/second and provided high-resolution visualization of crack propagation across the strike face. This technique was not used on the multi-hit and Lexan-only tests.

Residual velocities were measured using a Vision Research Phantom V7 monochrome high-speed camera. The frame rate was approximately 15,000 frames/second. A calibrated bar, located on the shot line during pre-tests, was used to scale the image. Software supplied with the camera then allowed for calculation of the residual velocity based on the frame rate and properly

[5] We will make no distinction in this report between V_{50} and V_{BL}; but, we will use V_{BL} to designate V_{50} as determined from Lambert's equation.

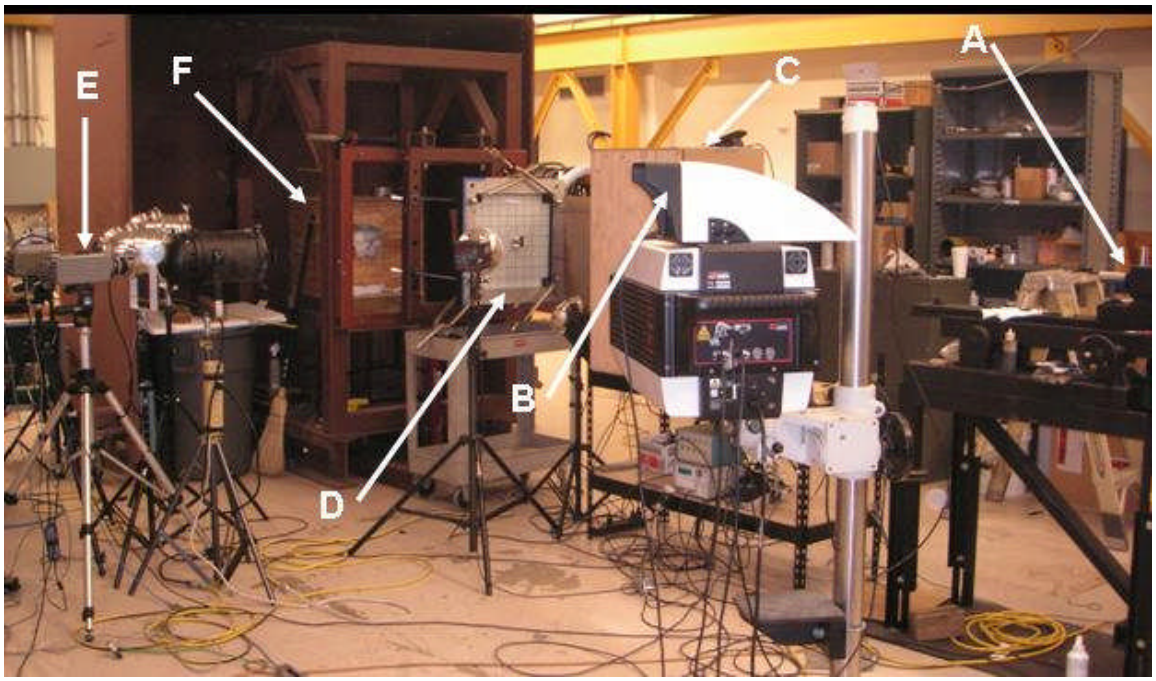

Figure 11. Typical range setup: A – universal gun; B – IMACON camera; C – velocity chronographs; D – target holder; E – residual velocity camera; F – "soft-catch" box.

scaled images. The residual velocity images were also used to confirm that the recovered projectiles were indeed in a similar condition to when they exited the back side of the glass sample.

Projectile lengths and masses were recorded before and after each test. Digital calipers and scales were used to record the pre- and post-test lengths and weights. A "soft-catch" box consisting of phone books, plywood, sand, and finally steel was used to stop the residual projectiles. After each test, the bullets were recovered from the catch box and numbered with the appropriate test number. Recovered projectiles were saved in plastic bags for further analysis. Occasionally, particularly at the higher impact velocities for the heavier bullets, the projectiles would pass through the recovery box and be stopped by a hard steel plate, generally causing damage to the bullet (camera images for determining V_r showed little or no damage to the bullet, but the recovered bullet exhibited considerable damage).

Targets were held in machined aluminum holders that supported the samples along all four sides, as shown in Fig. 12. Rubber pads were used to protect the samples from clamping stresses in each corner. A 2.5-cm x 2.5-cm grid was marked on the rear side of the samples to provide a scale in the IMACON images. Sometimes a thin sheet of white paper, taped to the rear of the target, was used to improve contrast for post-test photographs.

Figure 12. Target holder and clamps at corners with target specimen (strike face).

5.2 Lexan® Experiments

Sets of experiments were conducted to find V_s - V_r and V_{50} for the Lexan substrate. The results of these experiments provide an estimate of the penetration resistance of the Lexan, as well as data for validation of the polycarbonate material model for numerical simulations. The tabulated data are contained in Appendix A, and are plotted in Fig. 13. The 0.22-cal bullet could not be fired less than ~300 m/s because of friction between the skirt and the rifling. Nevertheless, since all the data agree quite well, it can be assumed that V_{50} for the 0.22-cal bullet is the same as for the other two bullets. The V_{50}'s, with the associated standard deviations, are summarized in Table 5. Lambert's equation—with p identically set to a value of 2.0—was fit through all the data, and is shown in Fig. 13.

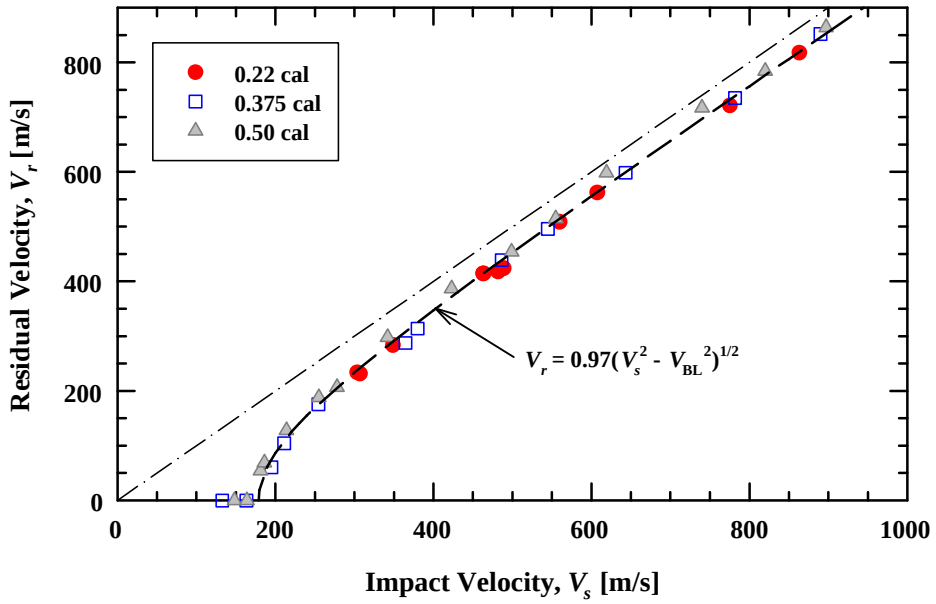

Figure 13. Residual velocity vs. impact velocity for Lexan targets.

Table 5. V_{50} Estimates for Lexan-Only Targets

Caliber	V_{50} (m/s)	Lambert V_{BL} (m/s)
0.22	–	179
0.375	175 ± 35	179
0.50	170 ± 17	179

5.3 Monoblock Glass Targets Experiments

Monoblock glass targets (targets with no backing substrate) were tested and the residual velocity versus the impact velocity recorded. A V_{50} could not be determined for the monoblock glass. A photograph of the front face of the damaged glass for a relatively low impact velocity (V_s = 257 m/s) is shown in Fig. 14(a). Five cracks run radially from the nominal impact point to the edge of the target, connected by cracks that propagated circumferentially. As was suspected, "gross" failure of the glass precluded the monoblock glass plates from stopping the bullet. A "spall cone" forms at the rear surface of the glass, denoted by the arrow in Fig. 14(b). This spall cone is probably the result of Hertzian cone crack formation that propagates to the rear surface of the target. With no substrate to prevent separation of the fractured glass, the failed glass is "blown" out of the target with the exiting bullet. High-speed video images show a cloud of glass debris, which obscures the exiting bullet until separation of the bullet from the glass debris downrange from the target.

(a) Front (strike) face. **(b) Rear (exit) face with spall cone.**

Figure 14. Photographs of the front and rear faces of a monoblock glass target experiment: 0.50-cal bullet (21-mm-thick Borofloat glass), V_s = 257 m/s.

There is a velocity dependence on the extent of cracking damage to the glass, as shown in Fig. 15. In general, the damage area and the number of cracks increases with impact velocity; although above ~550 m/s, the radial extent of damage tends to asymptote to covering most of the surface area of the target plate. In Figs. 15(c-d), a 2.5-cm square grid was marked on the rear surface of the glass prior to the experiment. A piece of paper was placed over the rear surface to improve contrast for the photographs.

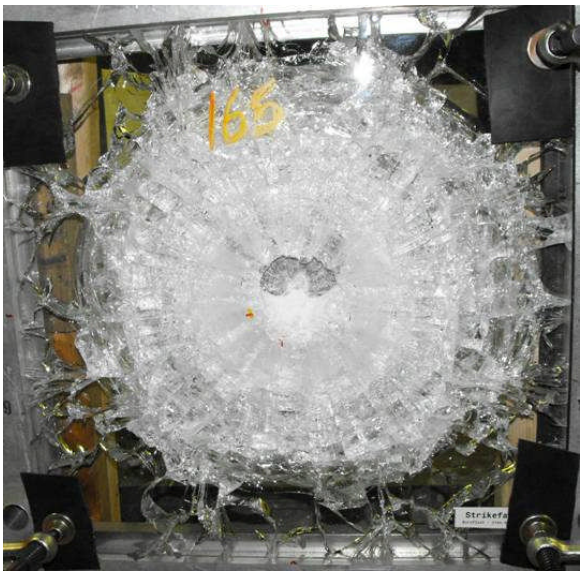

(a) V_s = 911 m/s

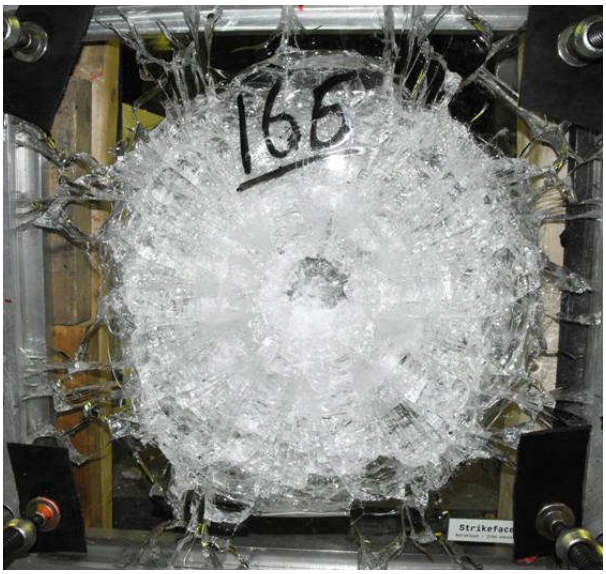

(b) V_s = 740 m/s

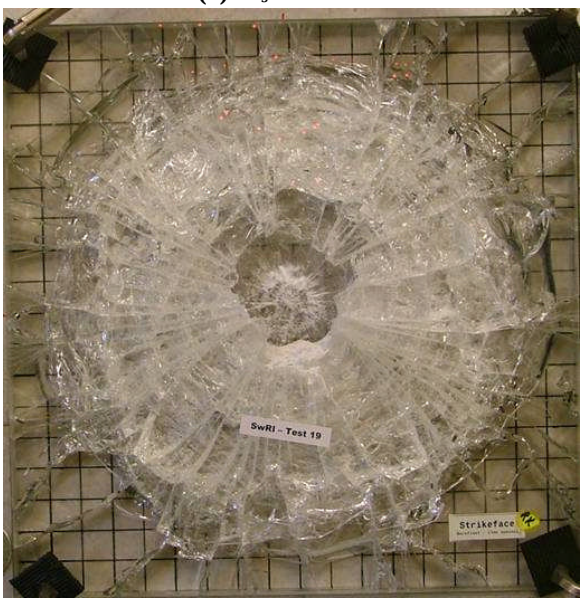

(c) V_s = 516 m/s

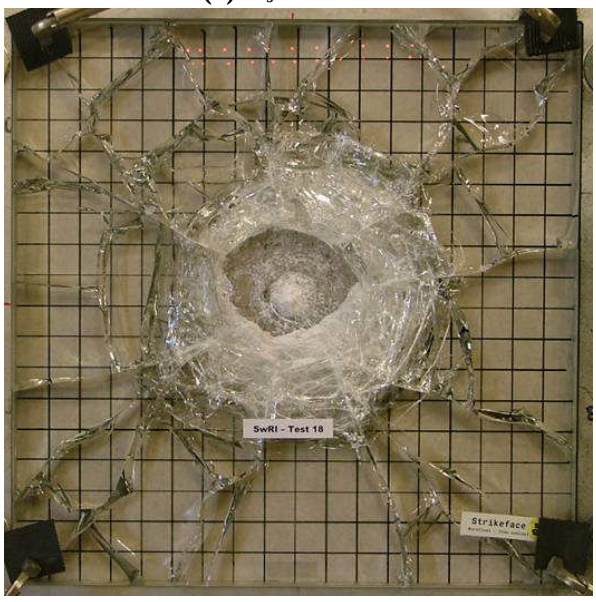

(d) V_s = 307 m/s

Figure 15. Glass damage as a function of impact velocity: 21-mm-thick glass, 0.50-cal bullet.

The residual velocity as a function of the impact velocity for the 21-mm-thick monoblock glass target (0.50-cal bullet) is shown in Fig. 16. The $V_s - V_r$ response appears to have two quasi-linear regions, with a distinct change in slope around 600 m/s. As will be shown later, this is approximately the velocity at which V_r begins to drop quickly towards zero when there is a Lexan substrate (that is, $V_s \sim V_{50} \approx 610$ m/s for the bonded glass targets). Thus, this change in slope is probably associated with the formation and failure of the spall cone. There is more scatter in the residual velocity for impact velocities below 600 m/s than above 600 m/s; nevertheless, the $V_s - V_r$ response is reasonably linear in the two regions. A linear least-squares regression line has been fit to the data in the two regions (above and below 600 m/s).

The response of the monoblock glass was qualitatively the same for the other two bullets (scales). However, there was a distinct difference in the quantitative response, as shown in Fig. 17 where monoblock data for all three bullets are plotted. At impact velocities below 600 m/s,

there is a definite trend that V_r, for the same V_s, is larger as the bullet caliber increases. Above 600 m/s, it is observed that the response of the glass target for the 0.22 cal bullet is distinctly different than for the other two bullets, which have approximately the same $V_s - V_r$ response. It is noted that results of curve fits depend upon which points might or might not be included in the data set for the regression analysis. For example, the 0.22-cal datum at ~650 m/s could be included with the lower velocity data (and not the higher velocity data), but the overall observation that the 0.22-cal monoblock targets have higher penetration resistance—that is, lower residual velocity for the same impact velocity—than the other two targets would remain valid.

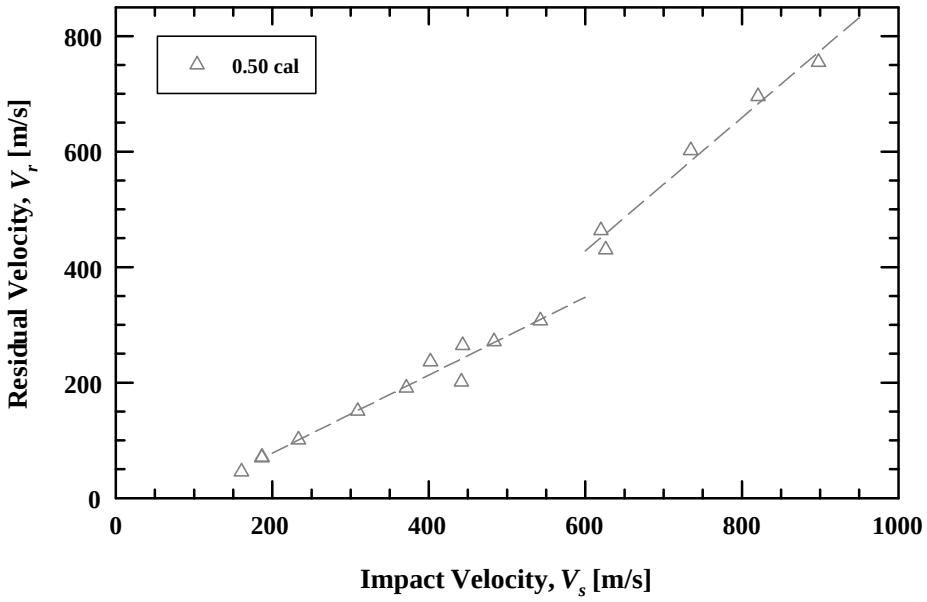

Figure 16. Residual vs. impact velocity for 0.50-cal monoblock glass target.

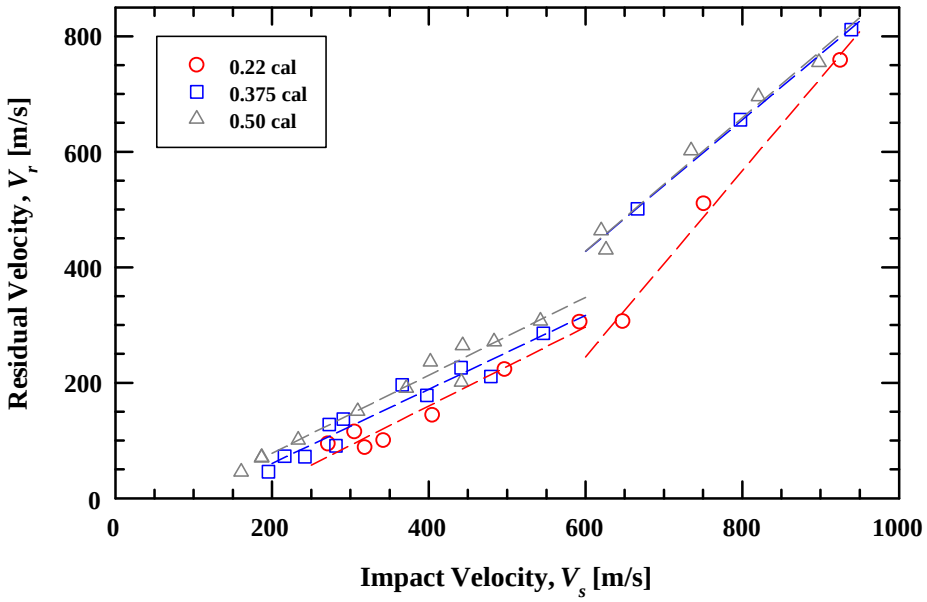

Figure 17. Residual vs. impact velocity for monoblock glass targets.

5.4 Bonded Glass Target with Lexan® Substrate

Two types of experiments were conducted with bonded glass. In the first set of experiments, each target was shot only once (impact was in the center of the target). The second set of experiments will be described in the next subsection.

It was shown in Fig. 15 that the areal extent of damage for the monoblock glass target increases with increasing impact velocity, although the damage extent tends to saturate by ~550 m/s. Damage to the front face of a bonded glass target and a monoblock glass target are compared at approximately the same impact velocity in Fig. 18. Although the extent of radial cracks is approximately the same, the area covered by circumferential cracks is much greater for the bonded glass target. Also, the extent of damage characterized by "opaqueness" is considerably larger for the bonded glass target. This may be due to damage induced by structural response (rebound) of the Lexan substrate.

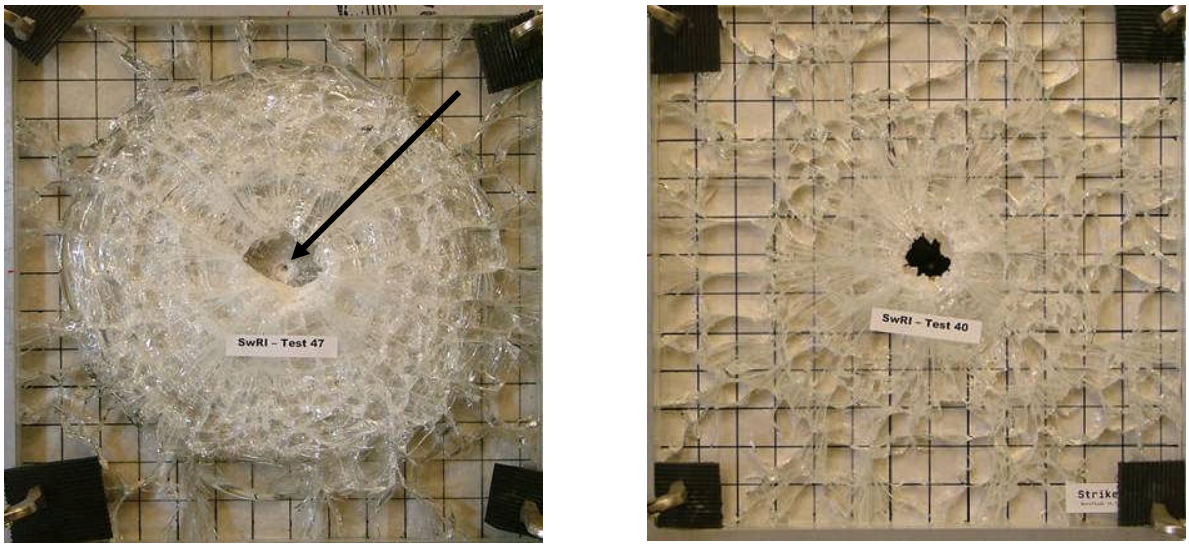

(a) Glass/Lexan: V_s = 645 m/s **(b) Monoblock glass: V_s = 662 m/s**

Figure 18. Comparison of extent of damage for bonded glass vs. monoblock glass.

A sequence of very high-speed images is shown in Fig. 19 for the front face of a 15.75-mm-thick bonded glass target and the 0.375-cal bullet. The impact velocity was 799 m/s; the residual velocity was 562 m/s. The "shadow-like" object in the foreground of the images is the make screen for triggering the camera (positioned approximately 12 mm in front of the glass target). The approximate time after impact is shown below each figure.

An average penetration velocity for calculating the time of perforation is: (799 + 562)/2 = 680 m/s. Thus, it takes the bullet nose approximately 23 μs to pass through the glass, and another 14 μs to pass through the Lexan substrate. The bullet tail exits the glass approximately 65 μs after impact. Glass damage appears to saturate by ~75 μs for this experiment (although not shown, damage continues to grow in extent between 65 μs and 75 μs, but with little or no further increase in damage at 85 μs). Comminuted glass is ejected from the target radially and somewhat back towards the gun barrel, obscuring the central region of damaged glass in several of the images. Ejection of the comminuted glass in the direction of the gun barrel is not as prevalent (and/or missing) in the high-speed images of the monoblock glass targets.

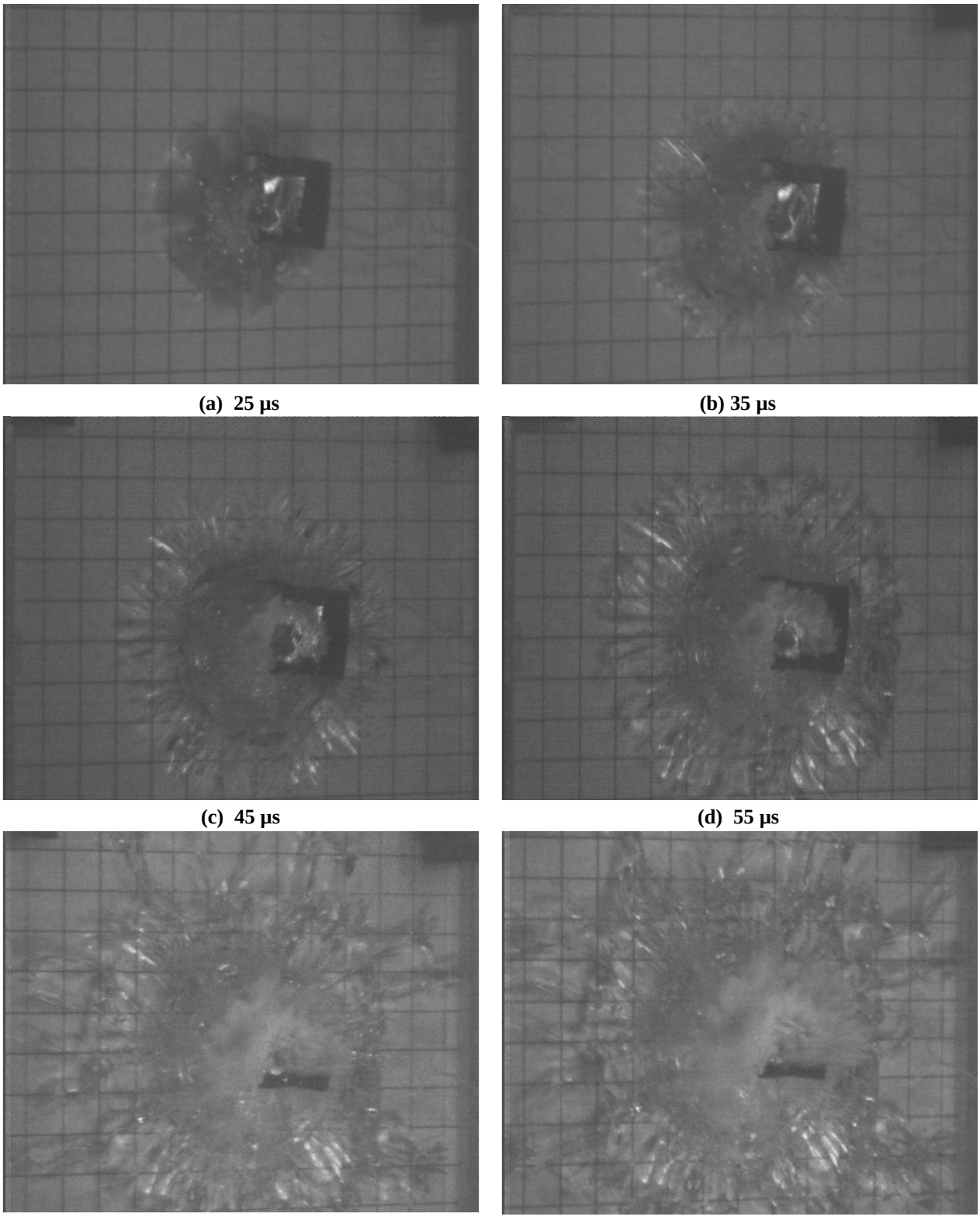

(a) 25 µs **(b) 35 µs**

(c) 45 µs **(d) 55 µs**

(e) 85 µs **(f) 105 µs**

Figure 19. Sequence of high-speed images of damage propagation (Test 29, V_s = 779 m/s) of a bonded glass target.

Figures 20 – 22 show the V_s – V_r response for the single-shot experiments with the three bullet calibers. Also plotted in each figure are the data from the corresponding scale monoblock glass experiments, that is, the data shown in Fig. 17. The V_s – V_r response of the monoblock glass lies a little above the bonded glass data for impact velocities above ~650 m/s. As expected, the residual velocity for the monoblock glass should be a little higher because the bullet does not have to perforate the Lexan substrate (see Fig. 13). For the bonded glass target, the Lexan substrate holds the damaged glass in place, and the glass/Lexan target can arrest the bullet at $V_s \approx 650$ m/s and lower.

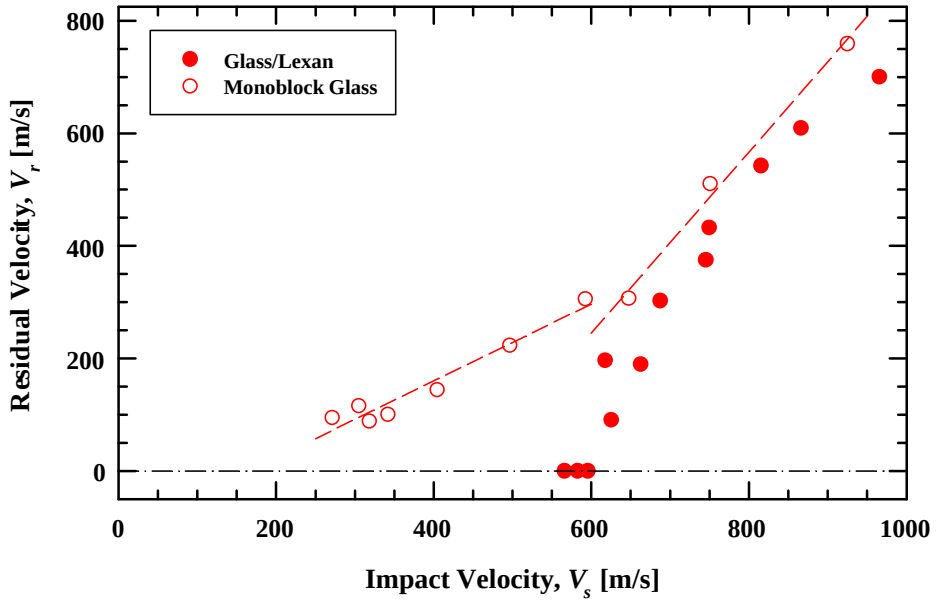

Figure 20. Residual vs. impact velocity for monoblock glass and bonded glass targets: 0.22-caliber bullet.

With regards to Figs. 20 – 22, it is not specifically the Lexan substrate that provides the increased penetration resistance of the bonded glass targets. This can be readily inferred from the response of Lexan-only targets (Fig. 13). Rather, it is the fact that the Lexan holds the glass in place, and the bullet now must penetrate damaged glass before reaching the Lexan substrate material. Without the Lexan, the damaged glass is easily pushed out in front of the bullet, offering effectively no "late-time" penetration resistance.

A distinct difference is observed in the response of the 0.22-cal bonded glass experiments compared to the 0.375-cal and the 0.50-cal experiments. The exit holes in the Lexan for the 0.37-cal and 0.50-cal experiments are slightly smaller than the diameter of the bullets.[6] The arrow in Fig. 18(a) points toward the hole in the Lexan for a 0.375-cal target. In contrast, the Lexan in the 0.22-cal experiments has a very large exit plug—with a diameter approximately 4 times that of the bullet—as shown in Fig. 23. The adhesive interlayer is visible in the photograph. Additionally, there are large radial cracks emanating from the circumference of the plugged region, highlighted by the arrows in Fig. 24. These radial cracks are reminiscent of petalling in thin, ductile targets. These phenomena were observed for all of the 0.22-cal glass/Lexan targets that were perforated (including each perforation for the multi-hit targets). In

[6] A pristine bullet cannot be pushed through the hole in the Lexan. The bullet opens a cavity in the Lexan as it penetrates into and through the substrate material. Some elastic rebound of the radially compressed material results in the final hole being slightly smaller than the caliber of the bullet that made the hole.

contrast, all of the perforated 0.375-cal or 0.50-cal bonded glass targets had a small exit hole in the Lexan.

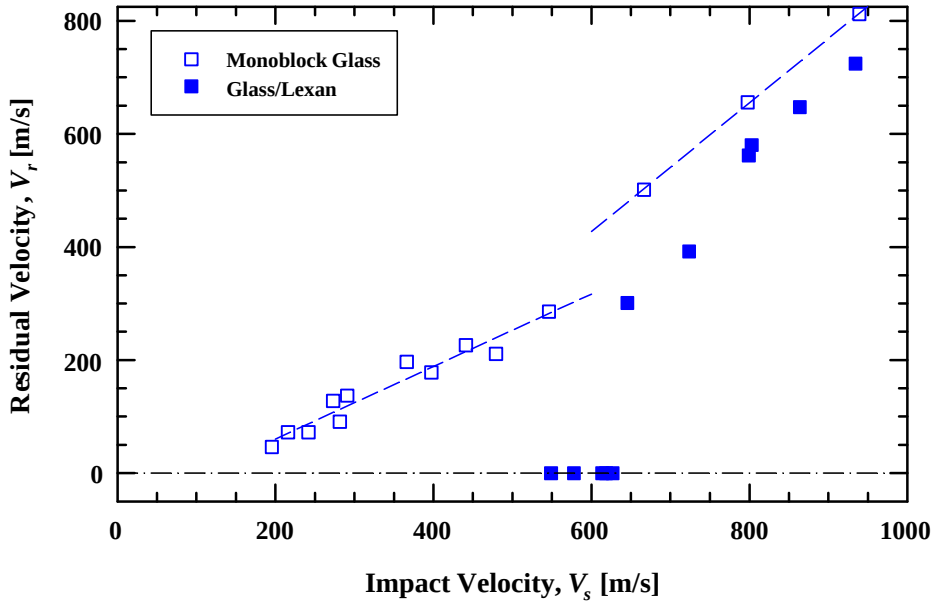

Figure 21. Residual vs. impact velocity for monoblock glass and bonded glass targets: 0.375-caliber bullet.

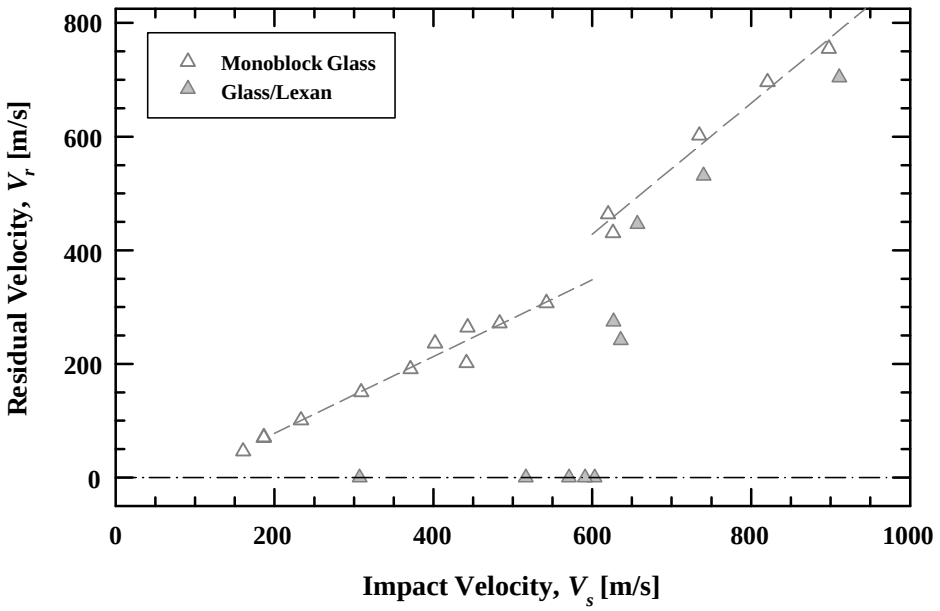

Figure 22. Residual vs. impact velocity for monoblock glass and bonded glass targets: 0.50-caliber bullet.

The difference in failure behavior of the bonded glass targets can be hypothesized to be the result of the time-dependent failure dynamics of the glass. For the 0.375-cal and 0.50-cal targets, sufficient time is available for damage to initiate and propagate in the through-thickness direction so that the bullet effectively penetrates into damaged glass. That is, the glass is more comminuted at homologous (scaled) times for the larger caliber targets and flows relatively

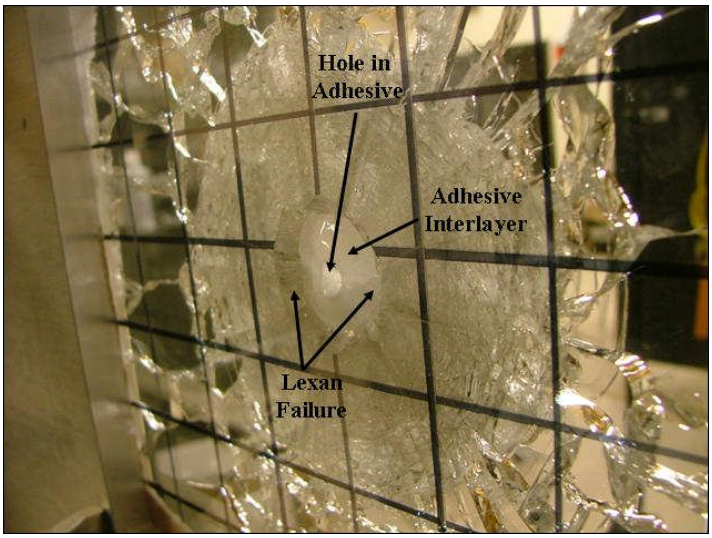

Figure 23. Lexan failure on rear side of 0.22-cal bonded glass targets.

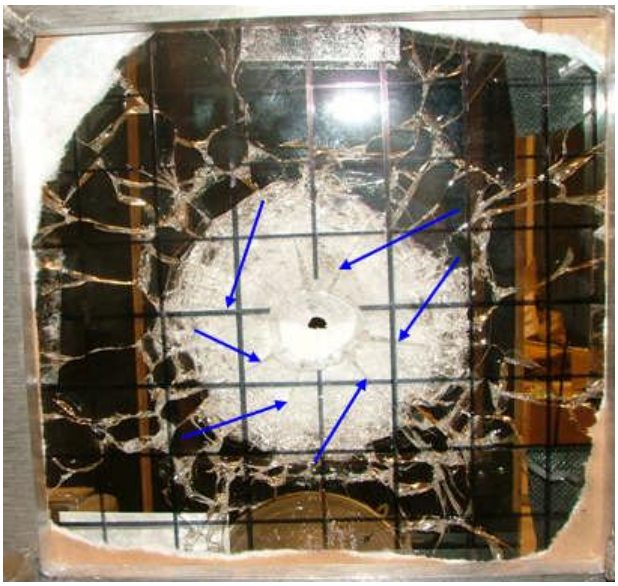

Figure 24. Petalling-like failure of Lexan substrate for 0.22-cal bonded glass targets; the arrows denote the petal-like cracks emanating from failure plug.

easily around the bullet.[7] With reference to Eqns. (1) and (2)—also see the scaling laws in Table 1—our hypothesis suggests that there was not sufficient time for the glass to be damaged in the through-thickness direction for the 0.22-cal bullet, and thus the bullet had to penetrate glass that has not been fully comminuted.[8] This glass "plug" then loads the Lexan substrate over a much larger area than the cross-sectional area of the bullet. It is well-known that "projectiles" with a

[7] Bullet loading and target response are different because of dissimilar damage (degree and extent) of the glass at homologous times for the three scale sizes. Thus, damage evolution results in overall dissimilar target response for the three target types.

[8] Fracture conoids, i.e., Hertzian cone cracks, may precede comminution evolution.

diameter considerable larger than the plate thickness will result in a petalling failure mode, exactly as observed for the 0.22-cal targets.[9]

This hypothesis also explains the qualitative difference in the residual velocity of the 0.22-cal bullet, compared to the 0.375-cal and 0.50-cal bullets, in the monoblock glass, as most readily observed in Fig. 17. Because the glass has not had sufficient absolute time to comminute fully, the 0.22-cal target offers more penetration resistance, particularly near V_{50}, than do the other two targets for their respective caliber bullets. These observations will be discussed further after discussing the multi-hit results.

5.5 Multi-Hit Bonded Glass Targets

As mentioned previously, there were two types of experiments conducted using the bonded glass targets. In the second series of experiments, each target was impacted 5 times. The first impact was in the target center, while the other four impacts were in the center of the four quads of the target, as shown in Fig. 25. For these multi-impact experiments, a Lexan cover was placed over the front surface (the Lexan front cover was clamped into place, but no adhesive was used) to preclude disintegration of the damaged glass. Circular holes, highlighted by the red circles in Fig. 25, were cut in the Lexan cover so that the bullet impacted directly onto the glass. The order of the shots, for all multi-hit experiments, was as follows: 1) target center; 2) upper left quadrant; 3) upper right quadrant; 4) lower right quadrant; and 5) lower left quadrant.

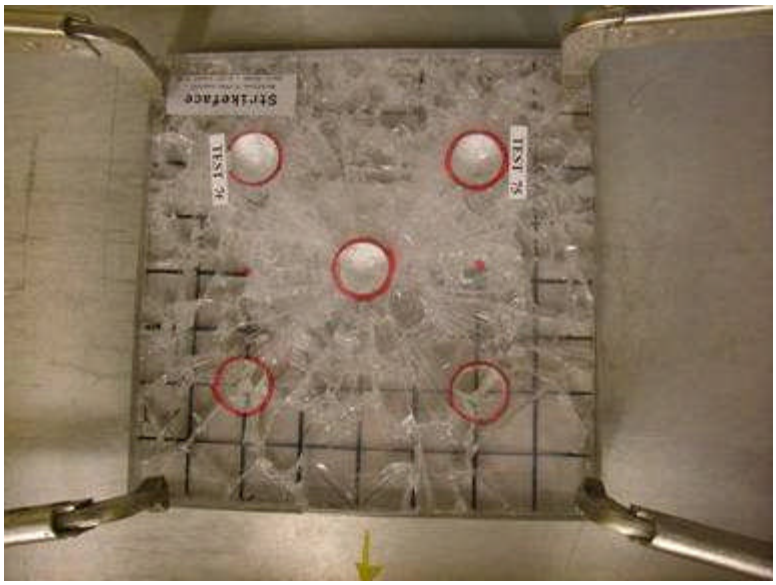

Figure 25. Multi-impact bonded glass target after three impacts.

Figures 26 through 28 show the $V_s - V_r$ response for the three targets. The shot number is next to the data point. Generally, the 1st, 2nd, and 3rd shots were nominally at the same impact velocity, while the 4th and 5th shots were at lower impact velocities (looking for a $V_r \sim 0$ m/s). It

[9] The loading of the Lexan substrate over a large diameter relative to the thickness results in the plate acting similar to a bulging membrane, creating large hoop stresses. These hoop stresses exceed the tensile strength of the Lexan, resulting in radial fractures. Formation of the radial cracks, combined with the exiting plug, removes the loading stresses on the membrane, and elastic forces cause the deformed Lexan plate to return to its nominally unloaded shape. Lexan, because of its limited ductility, cannot petal like a ductile metal target, but the loading and response are similar.

was realized that the first shot provided additional $V_s - V_r$ data for single-hit response (the solid symbols in the figures), and could be included with that data set. The impacts into the damaged glass—shots 2, 3, 4, and 5—follow a similar trend and can be grouped together. Therefore, the $V_s - V_r$ data are replotted in Figs. 29 – 31. The solid symbols denote the single-shot impact experiments or the first shot of the multiple-hit experiments. The open symbols denote data from shots 2 through 5 for the multiple-hit impact experiments. The dashed curves through the two sets of data points (the solid and open symbols in each graph) are regression fits to Lambert's equation, Egn. (5). These regression fits will be discussed in the next subsection.

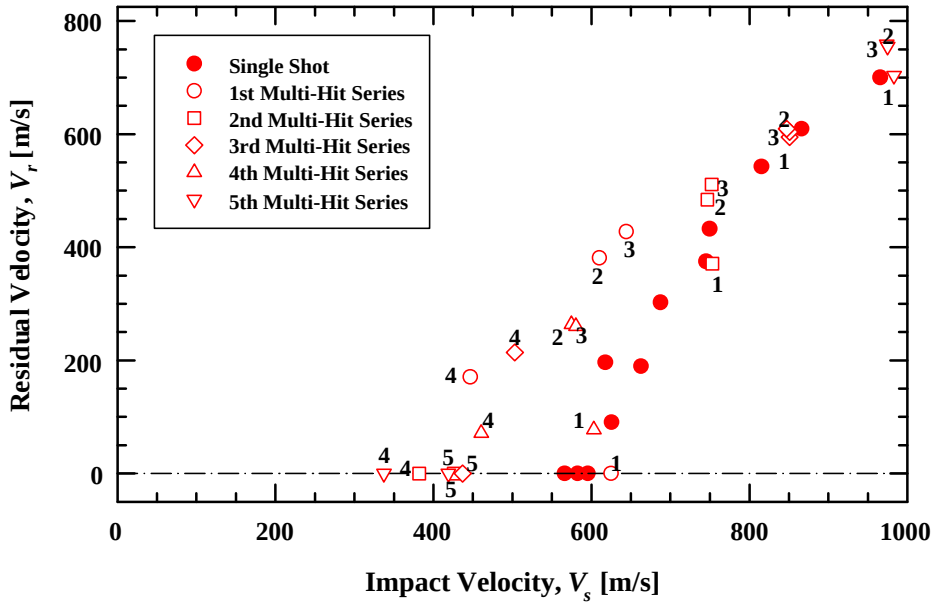

Figure 26. Multi-hit impact experimental results for 0.22-cal target.

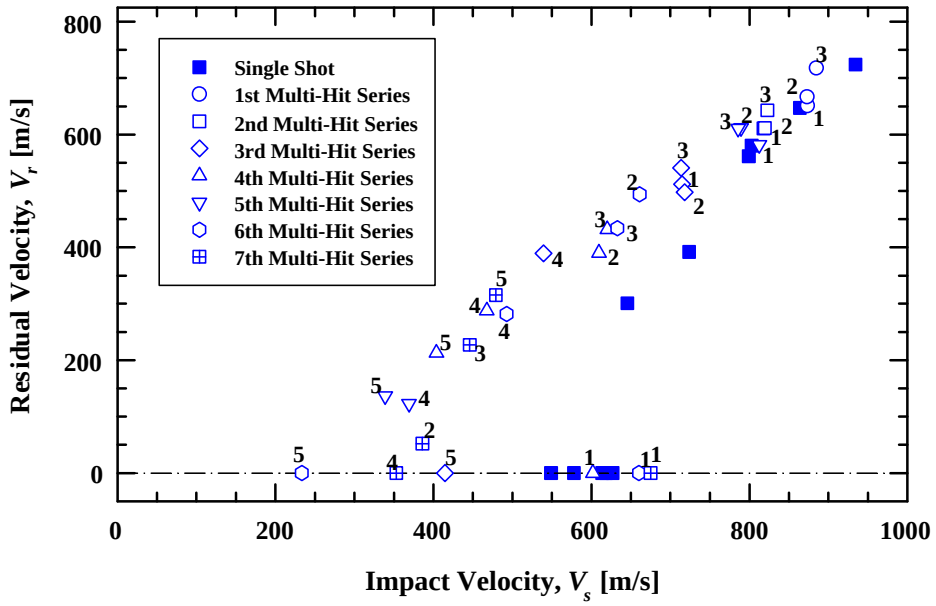

Figure 27. Multi-hit impact experimental results for 0.375-cal target.

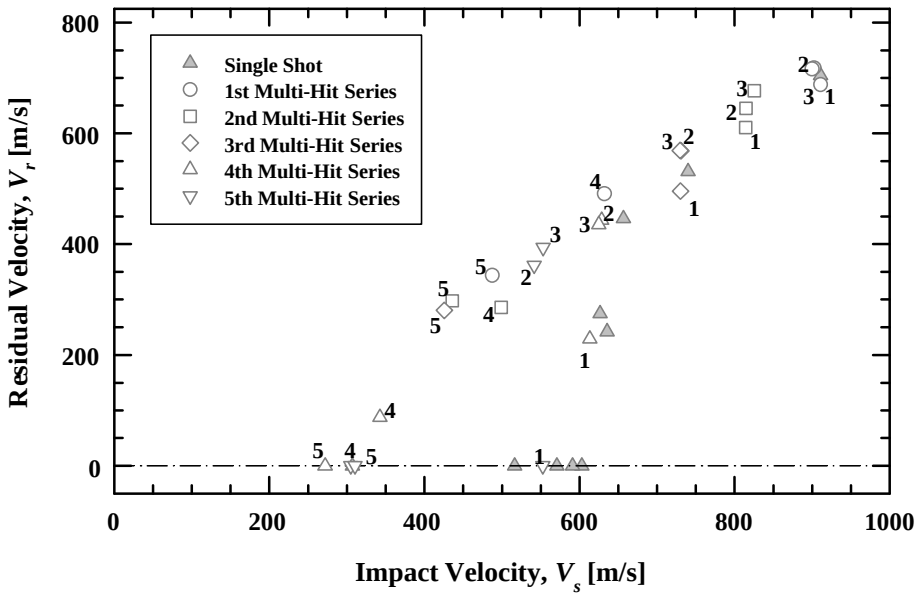

Figure 28. Multi-hit impact experimental results for 0.50-cal target.

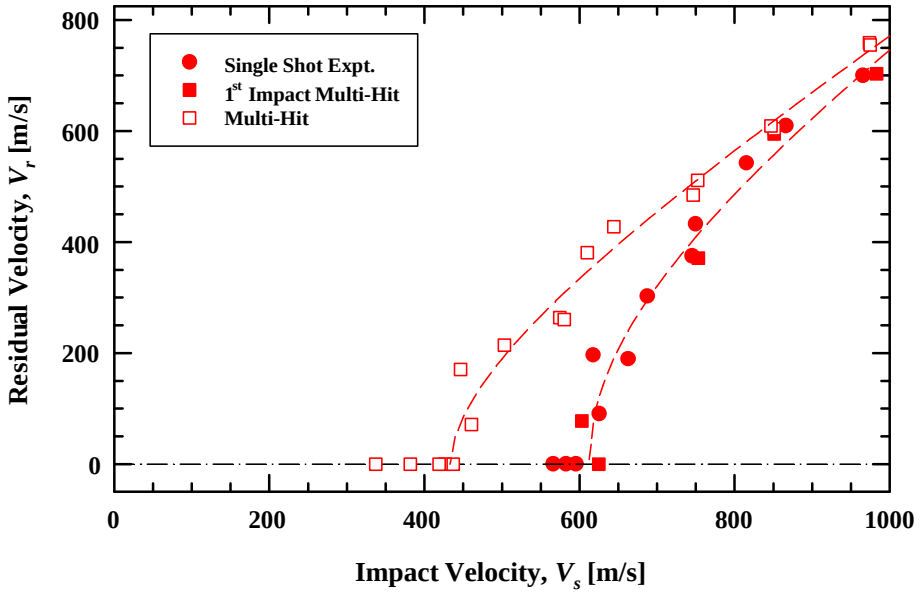

Figure 29. Impact into multi-hit glass vs. single-hit bonded glass: 0.22-cal target.

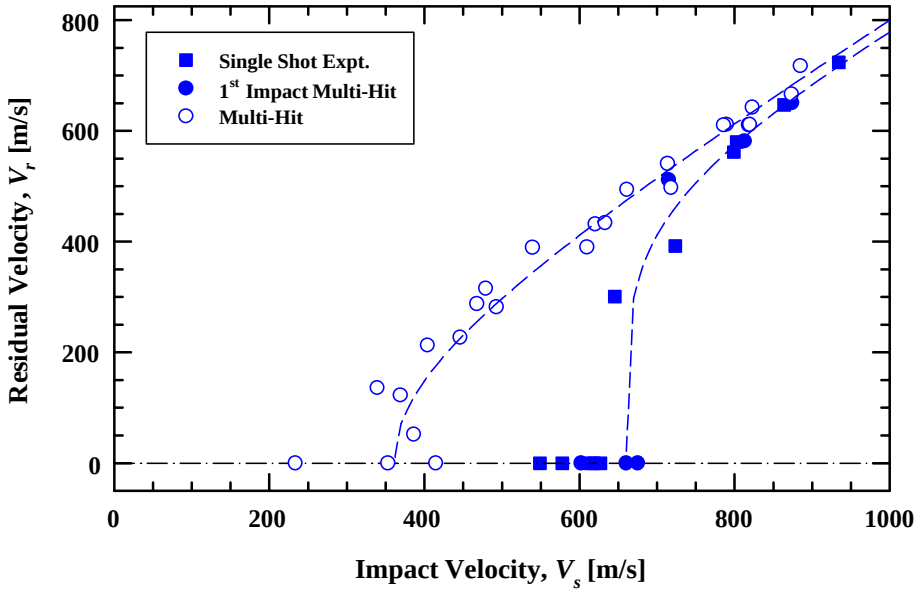

Figure 30. Impact into multi-hit glass vs. single-hit bonded glass: 0.375-cal target.

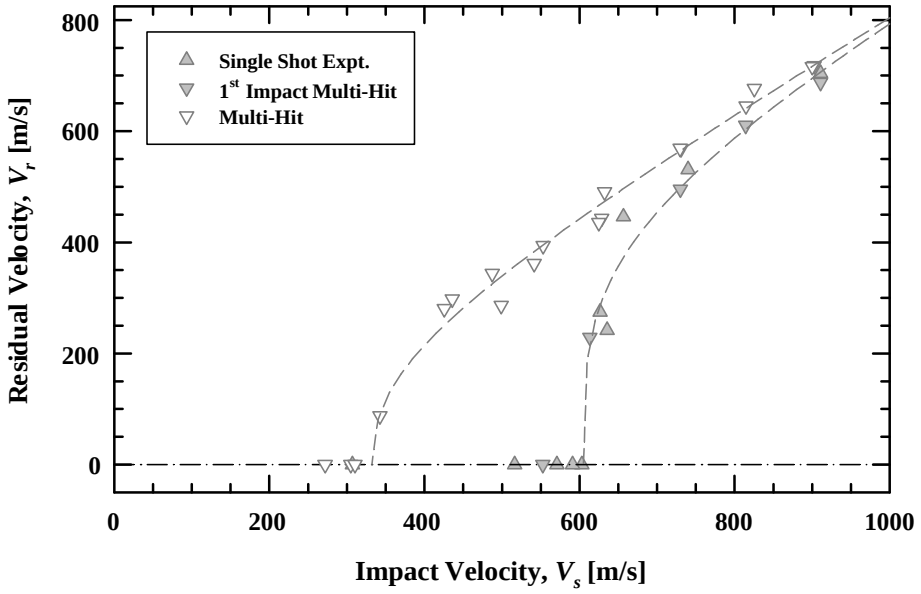

Figure 31. Impact into multi-hit glass vs. single-hit bonded glass: 0.50-cal target.

5.6 V_{50} Determination

V_{50} was determined using two methods: 1) averaging complete and partial penetrations, and 2) nonlinear regression analysis to Lambert's equation, Eqn. (5). For the first method, the two highest velocity partial penetrations and lowest two complete penetrations were averaged. A standard deviation (s) was also calculated. Because there could be a zone of mixed results, the velocity for some partial penetrations could be higher than complete penetrations; for example, see the open circles between V_s of 350 and 410 m/s in Fig. 30. For the second method, nonlinear regression analysis was performed on each data set shown in Figs. 29 – 31, for a total of six analyses. The fit parameters determined from the analyses are a, p, and V_{BL} in Eqn. (5). Often,

the exponent p is set to 2.0 (in which case, the Lambert equation is essentially a statement of conservation of energy). We conducted the regression analyses with p as a regression variable and with p fixed at 2.0, and then selected the best fit. V_{50} and V_{BL} results for the experiments are summarized in Table 6 and plotted in Fig. 32. In Fig. 32, the data points for V_{50} and V_{BL} are centered on the bullet caliber to enhance clarity.

Table 6. V_{50} for Single-Hit and Multi-Hit Impacts

Target	Single Shot or Multi-Hit	4-shot V_{50}		Lambert Equation		
		V_{50} (m/s)	s (m/s)	V_{BL} (m/s)	a	p
0.22	single shot	610	14	611.9	0.943	2.00
0.22	multi-hit	420	34	433.2	0.896	1.75
0.375	single shot	657	14	660.0	0.806	4.57
0.375	multi-hit	369	33	360.6	0.857	2.00
0.50	single shot	608	15	605.2	0.835	3.57
0.50	multi-hit	336	38	332.4	0.831	2.36

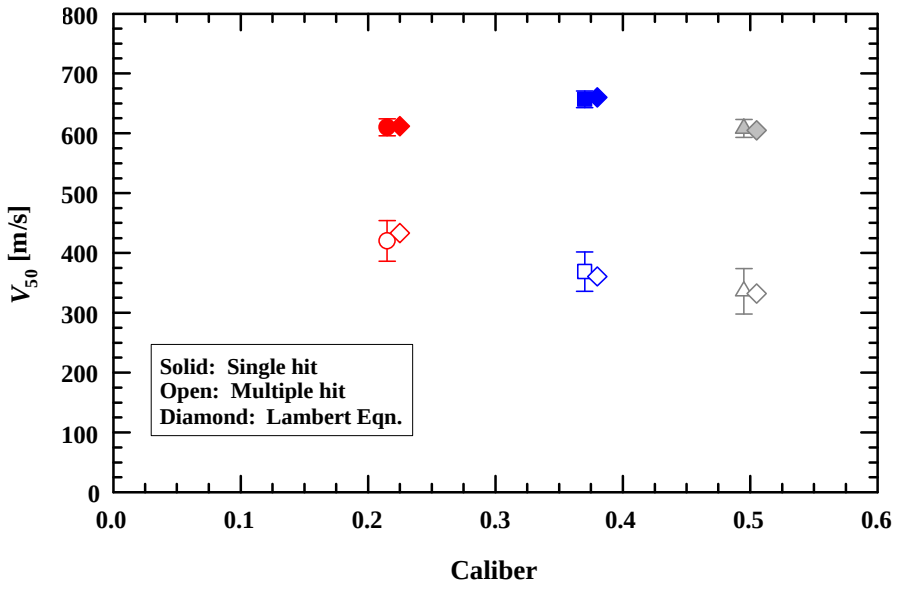

Figure 32. V_{50} vs. bullet caliber.

The standard error in V_{50} for damaged glass is approximately ±36 m/s, whereas for the intact (virgin) glass is approximately ±15 m/s. The nature of the multi-hit (damaged) glass probably precludes obtaining a tighter tolerance on V_{50}.

The agreement between V_{50} and V_{BL} is very good, providing confidence in the estimating procedures. For the damaged glass, there is a consistent trend that the smaller caliber targets have a somewhat higher ballistic resistance to penetration (higher V_{50}) than the larger caliber targets. This same trend was observed in Fig. 17 for the monoblock glass targets.

For the single-shot bonded glass targets, there is a reversal of the trend—for the 0.22-cal target—that the smaller caliber targets provide more ballistic resistance than the larger caliber targets. However, it has been noted that the failure mode for the 0.22-cal bonded glass targets, Figs. 23 and 24, was completely different than for the two larger targets. Structural bending of the 0.22-cal Lexan substrate, created by the forward motion of the glass being pushed by the

bullet, produces high radial and circumferential tensile stresses in the Lexan, which then fails "catastrophically" by plugging (along with radial cracks). This structural-induced failure results in a lower V_{50} than the more conventional failure observed for the 0.375-cal and 0.50-cal targets. The glass in the 0.22-cal targets, acting collectively to push against the Lexan, is consistent with an interpretation of less damage to the glass (in absolute time) for the 0.22-cal targets than for the larger targets.

In conclusion, the trend that V_{50} decreases with increasing scale size for the multi-hit glass, and the 0.375 and 0.50-cal bonded glass target, supports the hypothesis that damage nucleation and propagation in glass is time dependent. The change in failure mode exhibited by the 0.22-cal bonded targets complicates a comparison of the V_{50} data with the other scale sizes.

5.7 Bullet Erosion and Dwell

The bullets were weighed and their lengths measured prior to shooting. After each test, the residual bullet was removed from the soft-catch box, the length measured, and weighed. On some experiments, most notably the high-velocity shots with the more massive bullets, the bullets penetrated through the soft-catch media and hit the steel backup plate. Striking the steel plate resulted in additional damage to the bullet. Comparison of the recovered bullet with images in the high-speed video images permitted identification of those bullets that suffered damage from striking the steel plate. For these cases, lengths were estimated from the video images, but no reliable masses could be estimated; and thus, these mass data were not used in the following analysis.

One set of data—the 0.50-cal results—will be discussed in detail; then differences observed at the other scale sizes will be summarized. The normalized residual lengths, that is, the measured length of the recovered bullet divided by the initial length of the bullet (L_r/L_o), are plotted in Fig. 33. There are four sets of data: 1) single-hit bonded glass (solid triangles), 2) monoblock glass (open triangles), 3) the 1st impact of a multi-hit series into the bonded glass (inverted solid triangles), and 4) the remainder of the multi-hit impacts into the bonded glass target (inverted triangles with cross). The vertical dashed lines denote the V_{50}'s for the single-hit and multi-hit bonded glass targets. For clarity, V_{D50} will be used to denote and distinguish the ballistic limit for the multi-hit targets from the ballistic limit (V_{50}) of the single-shot targets.

There are a number of important features. The data indicate that there is dwell of the bullet on the glass. Dwell can be distinguished from high-speed erosion. High-speed erosion occurs when the penetration stresses greatly exceed the strength of the bullet and there is continuous failure (erosion) of the bullet material at the penetration front. The erosion rate for high-speed erosion increases with increasing impact velocity. In Fig. 33, there is very little erosion of the bullet for velocities greater than V_{50}, regardless of target type. Below V_{50}—ignoring for the moment the multi-hit data—erosion increases with impact velocity (i.e., L_r/L_o decreases), which is what is expected if the bullet is dwelling. The fact that there is dwell with these Rc53 projectiles shows that the intact glass is very strong. Note, however, that for striking velocities just a little above V_{50}, damage to the glass must occur very rapidly as there is little bullet erosion at these higher impact velocities.

In general, bullet erosion from the monoblock glass targets overlay the bonded glass results. However, there is a sharp increase in eroded length (decrease in L_r/L_o) for the bonded glass near and a little below V_{50}, in contrast to the monoblock glass. This difference in response is probably the result of the formation and ejection of the spall cone in the monoblock glass.

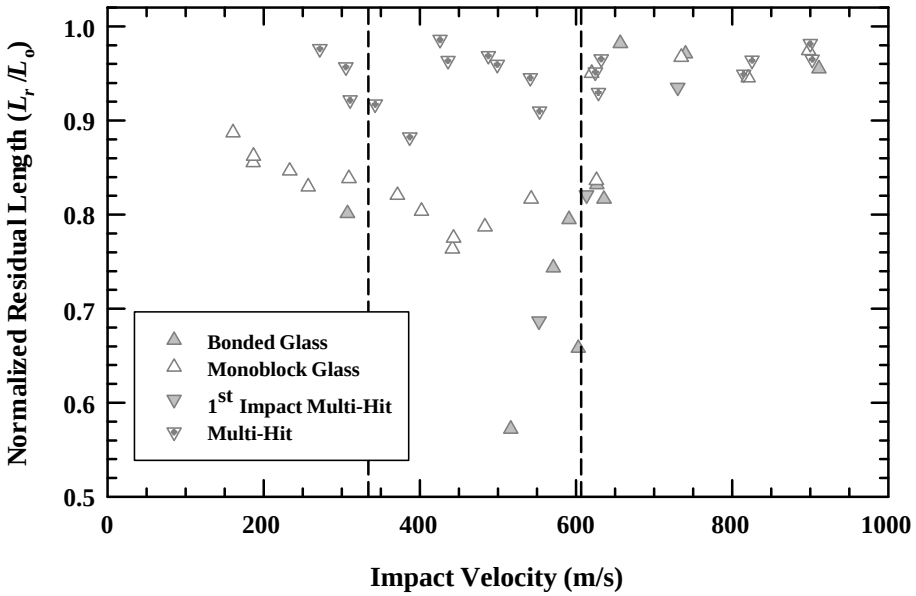

Figure 33. Normalized residual length vs. impact velocity for 0.50-cal bullet.

The data for the first shot of the multi-hit experiments are consistent with the single-shot bonded glass experiments. However, the remainder of the multi-hit experiments reveals two features of interest. Below V_{50}, the strength of damaged glass is significantly less than intact glass; that is, there is less erosion of the bullet. But similar to intact glass, the erosion rate does increase as the impact velocity approaches V_{D50}. But once $V_s > \sim V_{D50} + 50$ m/s, then L_r/L_o increases to a value that is approximately the same as for intact glass for $V_s > V_{50}$.

The normalized residual masses versus impact velocity are plotted in Fig. 34. There is a one-to-one correspondence to the data in Fig. 33, as expected, except for the cases where the bullet hit the steel plate in the catcher box (and the masses are not plotted). The normalized lengths show a larger decrease near V_{50} than the normalized masses because there is little mass

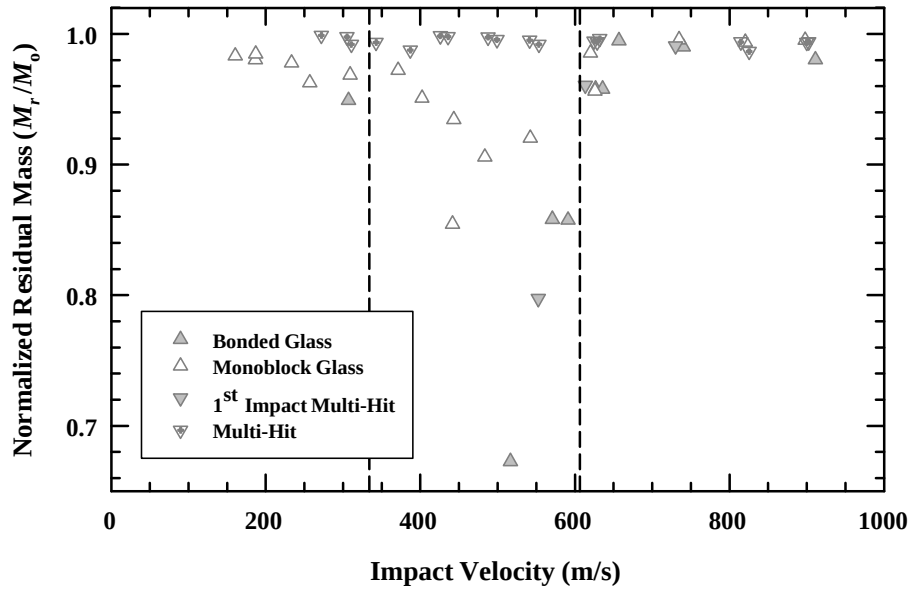

Figure 34. Normalized residual mass vs. impact velocity for 0.50-cal bullet.

associated with the initial erosion of the conical nose, as shown in Fig. 35. There is only 10% mass loss if approximately 30% of the bullet length is eroded. Therefore, Fig. 33 presents more readily useful information about the behavior of the glass since it provides directly an estimate of how long the glass retains strength for the bullet to dwell.

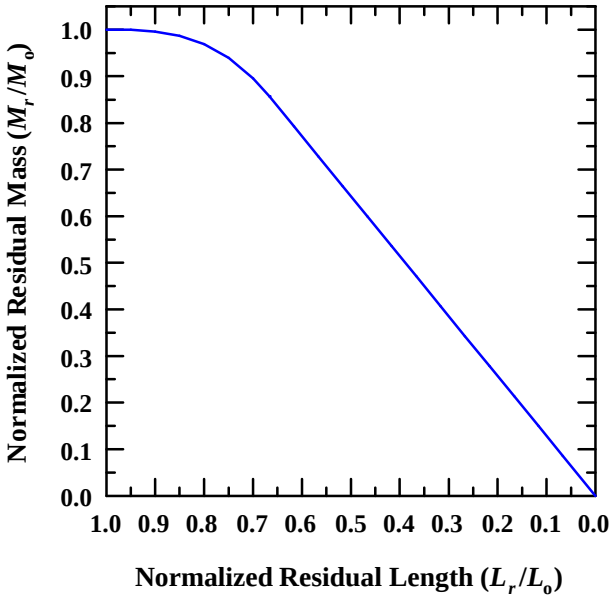

Figure 35. Normalized bullet mass vs. normalized length.

The observations and conclusions from Figs. 33 and 34 are:

1. The glass is very strong initially, resulting in bullet erosion, particularly near V_{50};
2. At approximately V_{50} + 50 m/s, there is very little erosion of the bullet for the single-shot targets;
3. Therefore, bullet erosion is caused by dwell, which persists until the glass is sufficiently damaged to result in penetration;
4. Above V_{50}, the glass must damage very rapidly after impact since there is little bullet erosion;
5. At approximately V_{D50} + 50 m/s, there is very little erosion of the bullet for the multi-hit targets;
6. Maximum bullet erosion (and dwell) is around V_{50} and V_{D50} for the single-shot and multi-hit targets, respectively;
7. Dwell time on the monoblock glass is less than dwell time on the bonded glass near V_{50}, probably because of the formation and ejection of the spall cone in the monoblock glass target;
8. Residual length is a more direct metric than residual mass (because the conical nose) for dwell/erosion.

As will be discussed below, a few of these observations are modified after examination of the 0.22-cal and 0.375-cal results.

Before proceeding, Orphal [25] conducted an analysis using the analytical dwell model of Anderson and Walker [26]. The model assumes that the penetration velocity is zero (that is, dwell), and then computes the projectile length and velocity as a function of time (the projectile velocity decreases due to deceleration). The model was applied to the monoblock glass targets since the assumption is that there is dwell until failure via the spall cone, at which point, there is no further penetration resistance.[10] Using this model and matching the experimental residual velocity, the dwell time can be estimated as well as the projectile residual length. The residual lengths from the model agree reasonably well with those measured experimentally for the monoblock glass targets. This analysis supports the argument that the bullet is dwelling on the glass.

The normalized residual lengths for the 0.22 bullets and the 0.375 bullets are shown in Figs. 36 and 37, respectively.[11] The same observations and conclusions reached relative to the 0.50-cal bullet results (Fig. 33) are applicable to the 0.22-cal and 0.375-cal bullets with the following notable differences:

1. Above V_{50}, dwell/erosion occurs (there is erosion) at higher impact velocities (0.22-cal and 0.375-cal bullets) than for the 0.50-cal bullet, but the time of dwell (amount of erosion) decreases with increasing impact velocity;
2. Below V_{50}, for the monoblock targets, the bullets appear to dwell somewhat longer (more erosion) as the impact velocity approaches V_{50} than for the 0.50-cal target. This would seem to imply that formation and ejection of the spall cone is taking somewhat longer to occur for the small bullets.
3. There is considerably more erosion of the 0.22-cal bullet for the multi-hit bonded targets as the impact velocity approaches V_{D50} than for the 0.50-cal bullet. The 0.375-cal bullet results lie in between the other two calibers.

For dwell, the erosion rate increases with increasing impact velocity (and in fact, without some other information—such as discussed relative to the sudden change in L_r/L_o above V_{50} for the 0.50-cal bullets—it would be difficult, then, to distinguish dwell from high-speed erosion). In Figs. 36 and 37, the amount of erosion decreases with increasing impact velocity above V_{50}. If the time interval for damage evolution is the same—independent of scale size—then the amount of erosion should have increased with increasing impact velocity; instead, the amount of erosion decreases with increasing impact velocity. This suggests that the damage rate might depend upon the overstress, as in Eqn. (2). Supporting this hypothesis are the observations that the failure front velocity is a function of the impact velocity [6], and that failure front propagation ceases if the driving stress is removed altogether [7-8]. Further, the failure front ceases to propagate if the distance between the failure front and the driving stress becomes too large [7-8]. These results have been interpreted to mean that failure requires a specific overstress at the failure front.

[10] There would be further deceleration of the projectile during penetration of the bonded (failed) glass targets, and thus, there would not be a one-to-one correlation between the residual velocity and residual length.

[11] The residual bullet masses are not plotted since it was concluded that the residual lengths provided more direct information concerning dwell/erosion.

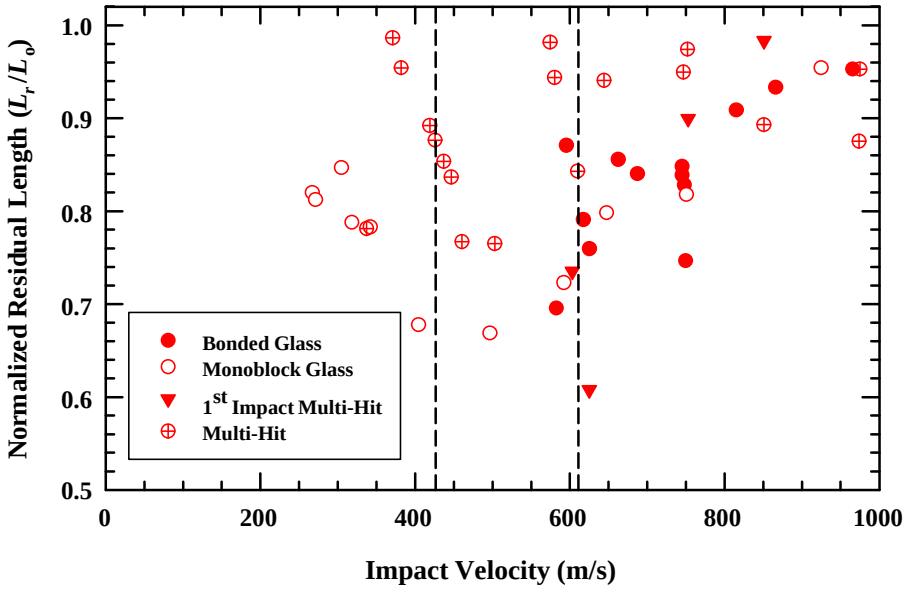

Figure 36. Normalized residual length vs. impact velocity for 0.22-cal bullet.

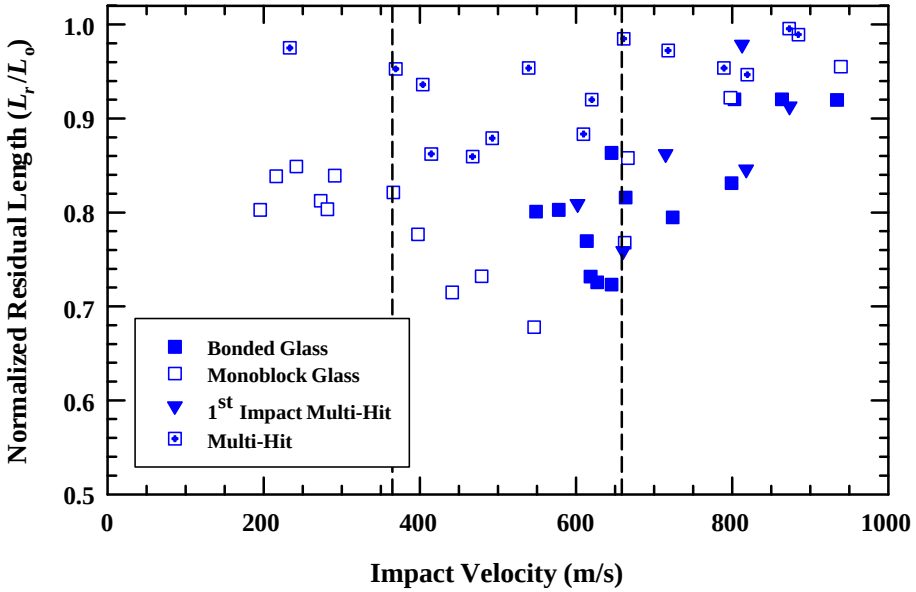

Figure 37. Normalized residual length vs. impact velocity for 0.375-cal bullet.

The normalized residual lengths for the three bullet calibers into the monoblock glass targets are compared in Fig. 38. The vertical dashed lines denote the V_{50} velocities for bonded glass for the three different caliber bullets. Below 300 m/s, the results overlay within the data scatter.[12] As long as the glass retains it strength to induce bullet dwell, then the results should be independent of scale size. But between ~400 m/s (and possibly as low as ~325 m/s) and 550 m/s—the data points within the rectangular box in Fig. 38—a definite trend emerges,

[12] It is V_{50}'s for the bonded glass targets that are relevant in this graph because it is at ~V_{50} for the bonded targets that the response of the monoblock glass targets deviate from the response of the bonded glass targets (Fig. 17).

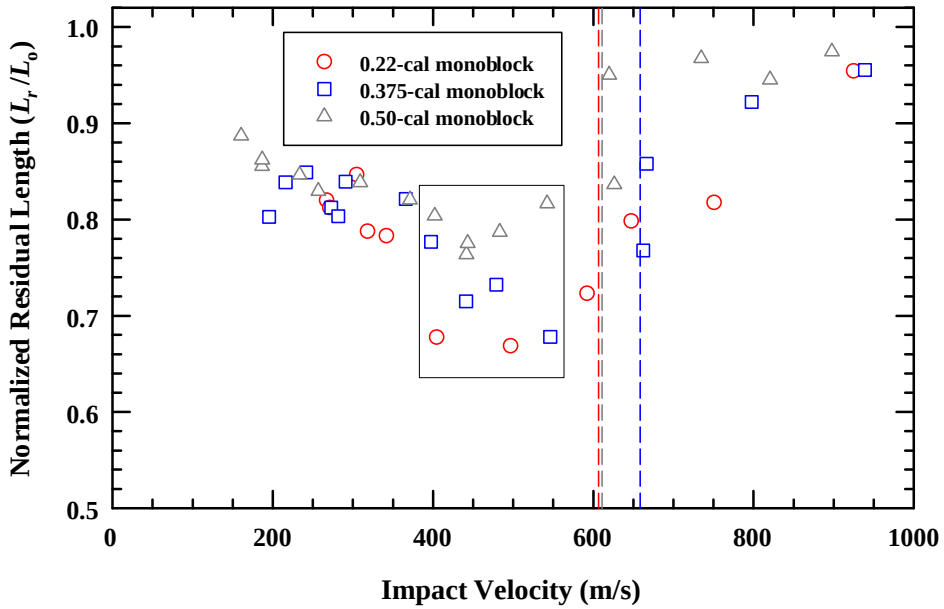

Figure 38. Comparison of normalized residual lengths for monoblock glass targets.

where dwell time (and thus eroded length) decreases with increasing caliber, again supporting the hypothesis that damage evolution is time dependent. Taken at face value, there is fundamental information "buried" within this data set. Evidently, time is sufficiently long at impact velocities lower than ~300 m/s that local damage can fully evolve (the strength of the glass remains sufficiently high to induce dwell) and the mechanical dynamics is independent of scale size. Nevertheless, the ballistic resistance of the damaged glass remains a function of scale size, as seen in Fig. 17, for these low impact velocities. Numerical simulations have shown that the extent of damage can affect penetration resistance [27]. Therefore, one possibility is that the spatial extent of damage is different at homologous times—for example, the formation of spall cone—resulting in higher ballistic resistance for the smaller scaled bullets.

Considerable variability is observed in L_r/L_o in the neighborhood of V_{50}, which is also complicated by the change in the failure mode of the 0.22-cal target. But for impact velocities above V_{50}, the same trend is observed, i.e., penetration resistance increases as the bullet caliber decreases. An important distinction needs to be made here. Although the eroded length decreases as the impact velocity increases, suggesting that damage rate is a function of overstress, there is also a time constant associated with damage evolution (for example, $e^{-t/\tau}$, were τ is a characteristic relaxation time). There would be no separation of the data for the three caliber bullets if there was not an absolute time dependency in damage nucleation and growth. *Thus, the experimental data suggest a combination of two effects: time-dependent damage nucleation that is a function of the overstress.*

The normalized residual lengths of the 0.22-cal and 0.50-dal bullets are compared for the bonded and monoblock glass targets in Fig. 39. The abscissa has been expanded to focus on impact velocities above V_{50}. As already observed, it is evident that the 0.22-cal bullet undergoes more erosion at the same impact velocity than does the 0.50-cal bullet above V_{50}. (There is considerable scatter in results below and slightly above V_{50}, but in general, the same trend holds.) As already observed, the 0.50-cal data show little variation in dwell time above V_{50}. However, the 0.22-cal data show decreasing target resistance as the impact velocity increases, perhaps converging with the 0.50-cal data at approximately 950 – 1000 m/s.

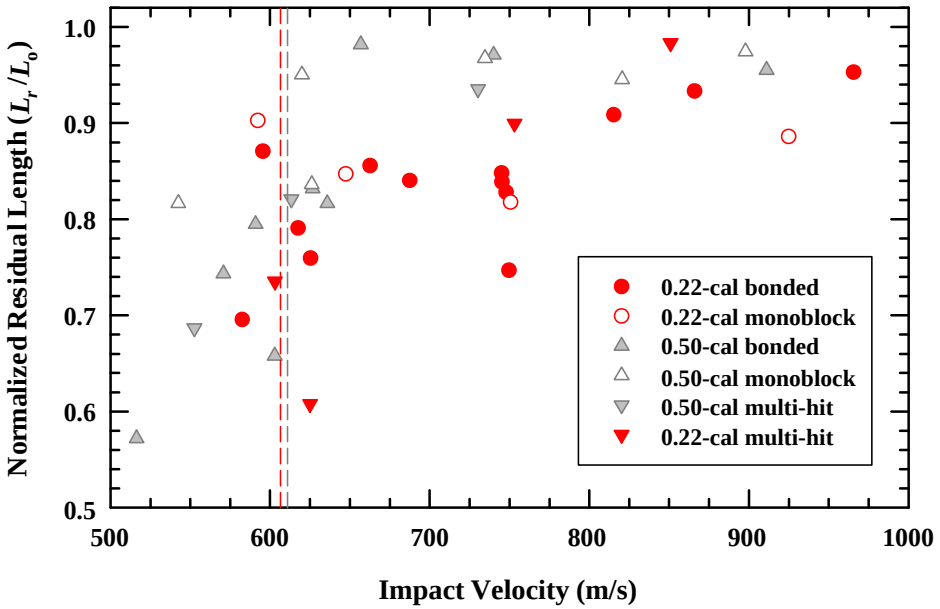

Figure 39. Comparison of normalized residual lengths for 0.22-cal and 0.50-cal bullets.

A comparison of the 0.375-cal data to the 0.50-cal data results in the same observations as described for Fig. 39. However, a comparison of the 0.22-cal and the 0.375-cal results, shown in Fig. 40, appears to indicate no scale dependence, within data scatter, between these two scales. However, it is not clear if the comparison should be made at the same impact velocities or at impact velocities relative to their respective V_{50}'s. The normalized residual lengths are plotted as a function of a normalized impact velocity, V_s/V_{50}, in Fig. 41. Although there is scatter, it is clear that the 0.50-cal bullet undergoes little erosion for $V_s > V_{50} + 50$ m/s, whereas the other two bullets continue to erode, but the erosion diminishes with increasing impact velocity. Also, although erosion of the 0.22-cal and 0.375-cal bullets is similar at the same

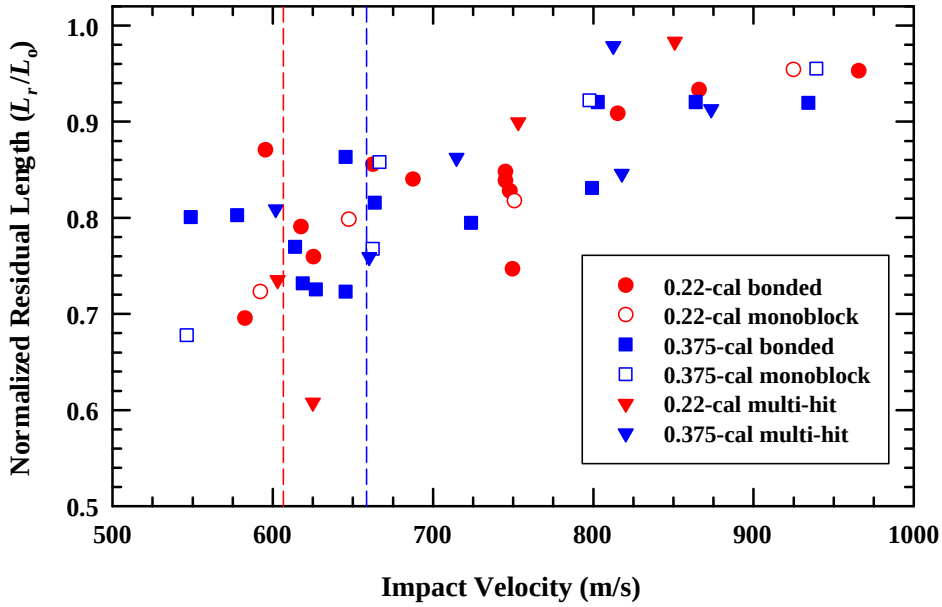

Figure 40. Comparison of normalized residual lengths for 0.22-cal and 0.375-cal bullets.

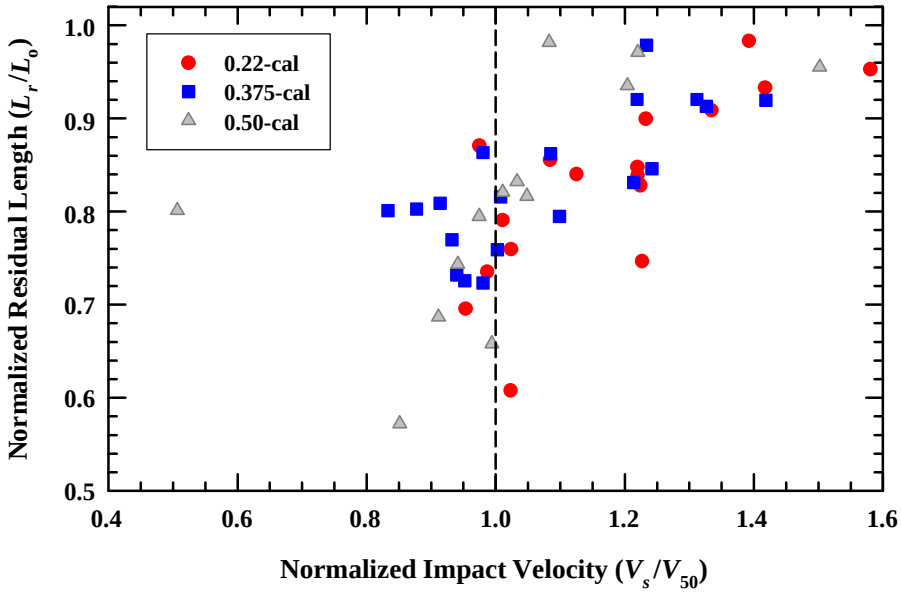

Figure 41. Normalized residual length vs. normalized impact velocity for bonded glass targets.

normalized impact velocity, there is a tendency for perhaps slightly more erosion of the 0.22-cal bullet.

The normalized residual lengths versus normalized impact velocity for the multi-hit targets are shown in Fig. 42. It is quite evident, even with the scatter, that there is a scale effect with dwell/erosion increasing as bullet caliber decreases.

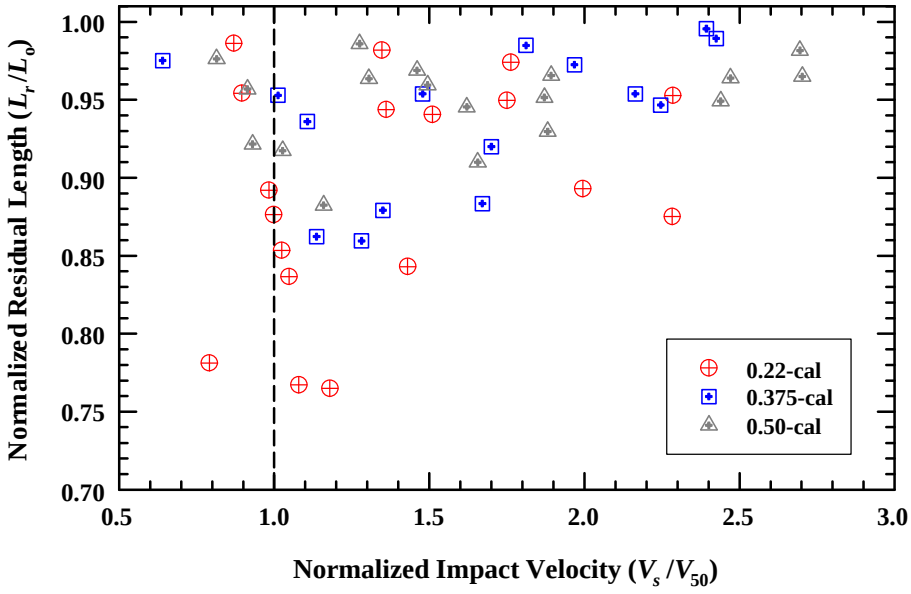

Figure 42. Normalized residual length vs. normalized impact velocity for multi-hit targets.

6.0 Summary and Conclusions

Glass impact experiments were designed at three different scales—0.22-cal, 0.375-cal, and 0.50-cal—named after the diameter of the bullets. Conical nose bullets were designed and heat treated to a hardness of Rockwell Rc53. Four experimental series were conducted at the three scale sizes:

- Lexan-only experiments;
- Monoblock glass experiments;
- Single impact bonded glass experiments (glass thickness the same as the monoblock glass, but bonded to a Lexan substrate);
- Multi-hit experiments (same target as the single-impact bonded glass experiments, but with 5 total impacts).

The experiments were conducted to obtain residual velocity as a function of impact (striking) velocity, including sufficient partial penetrations to calculate a V_{50}. The $V_s - V_r$ data were fit to the Lambert equation, Eqn. (5), to obtain another estimate of V_{50}.

The objective of the experiments was to investigate whether a time dependency exists in glass damage/failure for ballistic experiments, and if so, try to quantify this dependency. Although it is known that nucleation, growth, and propagation of damage are time dependent in general, the issue here is whether this time dependency can be observed in representative ballistic impact experiments. Damage evolves in absolute time, but time scales by the scale factor in the experiments. For example, damage may evolve as a function of (t/τ), where t represents the absolute time and τ is a time constant. However, for a model target that has a scale of ½ compared to the prototype target, scaled time is ½ of the prototype time. Thus, damage will have time only to evolve to $t/(2\tau)$ in the model as compared to the prototype at homologous times. If the time constant τ is sufficiently small, then damage saturates very quickly, and the model and prototype will have similar responses; otherwise, a "scale effect" will be observed. With respect to the ballistic experiments, if damage evolution is time dependent in the timeframe of the experiments, then the smaller scale targets will look "tougher," that is, have higher penetration resistance, than the larger scale targets; and this will be evident, for example, in increased erosion of the bullet and/or residual velocities and V_{50}.

No scale effect was observed in experimental results for the Lexan-only experiments. But a variety of scale effects were observed in the glass impact experiments.

There are clear differences between the penetration response of the 0.22-cal targets and the 0.50-cal targets. In general, the response of the 0.375-cal targets falls between the responses of the other two target scales.

The following summary highlights the *general* trends observed in the experimental data.

1. The trend for $V_s - V_r$ is that, for the same impact velocity (V_s), the residual velocity (V_r) is less as the bullet caliber (scale size) decreases, as shown in Fig. 43.
2. The V_{50}'s for multi-hit targets are considerably less (~1/2 to 2/3) than the V_{50}'s for a single-hit bonded target.

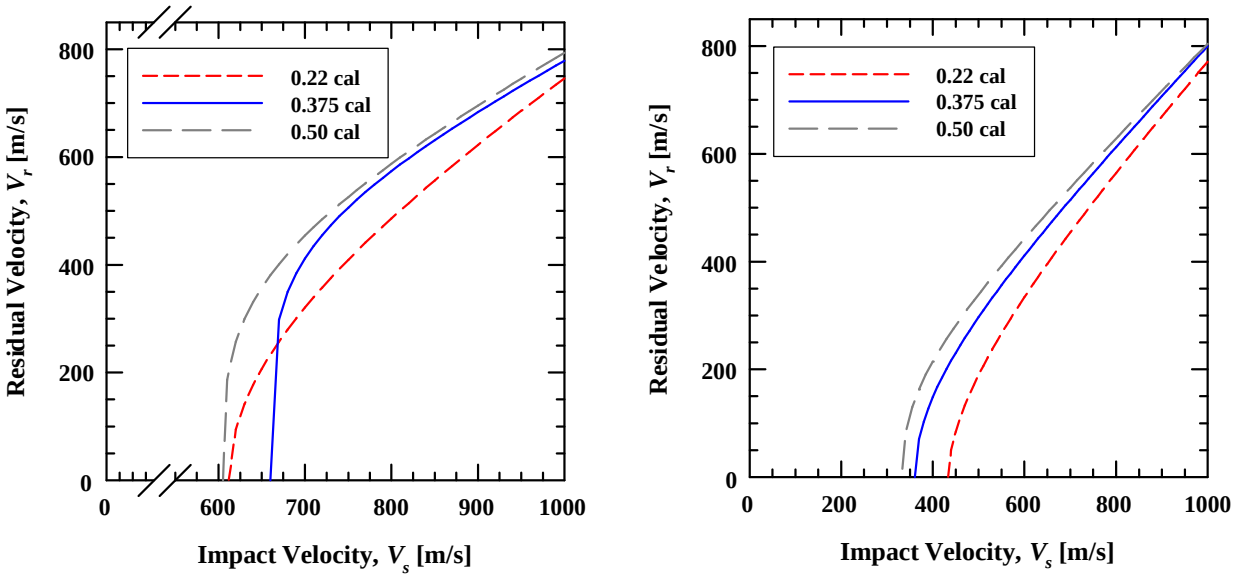

(a) Bonded glass targets. **(b) Multi-hit bonded glass targets.**

Figure 43. $V_s - V_r$ response for glass targets (Lambert's equation).

3. V_{50} for the 0.50-cal bullet into the bonded glass targets is less than that for the 0.375-cal target, Fig. 43(a). Although the high-velocity (>700 m/s) $V_s - V_r$ data for the 0.22-cal target suggests that it should have a higher experimental V_{50} than observed, the failure mode of the Lexan substrate was completely different for the 0.22-cal target (see Figs. 23-24 and discussion with these figures).
4. For $V_s > V_{50}$, the $V_s - V_r$ response of the monoblock targets parallels that of the bonded glass targets. But for V_s near V_{50} and below, the formation and ejection of a spall cone results in very low to no penetration resistance in the monoblock targets.
5. Bullet erosion is another good metric for examining the response of glass to bullet impact.
6. The glass is very strong initially, resulting in bullet dwell and erosion, particularly near V_{50}; bullet erosion is caused by dwell, which persists until the glass is sufficiently damaged to result in rigid-body penetration.
7. In these experiments, there is a scale (size) effect in bullet erosion; in general, erosion decreases as bullet caliber increases. This suggests that the time of erosion, and hence, damage evolution, is a function of scale size.
8. Generally, the monoblock glass results overlay, within the scatter, the bonded glass results for dwell, except that dwell time for the monoblock glass is shorter than for the bonded glass near V_{50} because of formation and ejection of a spall cone.

9. Maximum bullet erosion (and dwell) is around V_{50} for the single-hit bonded targets. For the multi-hit targets, maximum bullet dwell is around V_{D50}.

10. At approximately V_{50} + 50 m/s, there is very little erosion of the bullet for the 0.50-cal bullet. However, dwell continues for the 0.22-cal and 0.375-cal targets at velocities greater than V_{50}, but with the time of dwell decreasing (i.e., L_r/L_o increasing) with increasing impact velocity. Although there is scatter in the data, it appears that all targets have approximately the same dwell times at ~1000 m/s.

The above observations are consistent with a time dependency associated with failure of glass, and that this time dependency occurs on the time scale of ballistic impact. It also appears that the rate of damage is a function of the overstress. Hints of some of these phenomena were observed in reverse ballistic experiments, such as discussed in Refs. [6-8]. Observations on dwell transition velocities for borosilicate glass [9-10] also provide additional insights. For example, glass may still be intact beneath the penetrator (dwell), but Hertzian cone cracks can form at the perimeter of the projectile-target interaction zone. This has been observed in glass and ceramics [6,9,28]. Thus, characterizing damage with a single damage parameter may be overly simplistic and not permit capturing all the observed phenomena. As a robust glass model is currently under development, it remains to be seen what is necessary to replicate ballistic experiments into glass with reasonable fidelity.

It seems that there may be further information contained within the experimental data described here to glean additional insights about time constants and threshold stresses for a glass damage model, particularly if combined with some of the other experimental work that has been done with glass. This remains an active area of research at this time.

7.0 Acknowledgements

The authors would like to thank Dr. Douglas Templeton and Mr. Rick Rickert of RDECOM-TARDEC for their technical, administrative, and financial support of this research effort. We also thank Mr. Arthur E. Nicholls for conduct of the characterization experiments on the heat treated 4340 steel. The authors are very thankful for the comments and suggestions provided by Mr. Dennis L. Orphal (International Research Associates, Inc.) and Mr. Timothy J. Holmquist (Southwest Research Institute) in their reviews of the report.

8.0 References

1. Anderson CE Jr., Orphal DL, and Templeton DW. Reexamination of the requirements to detect the failure wave velocity in SiC using penetration experiments. ***Shock Compression of Condensed Matter–2003*** (Furnish MD, Gupta YM, and Forbes JW, Eds.), CP706, pp. 707-710, AIP, Melville, NY (2004).

2. Behner T, Anderson CE Jr., Orphal DL, Hohler V, Moll M, and Templeton DW. The failure kinetics of high density DEDF glass against rod impact at velocities from 0.4 to 2.5 km/s. *Proc. 22nd Int. Symp. Ballistics*, **2**: 877-887, DES*tech* Publications, Inc., Lancaster, PA (2005).

3. Orphal DL, Behner T, Hohler V, Anderson CE Jr., and Templeton DW. Failure wave in DEDF and soda-lime glass during rod impact. ***Shock Compression in Condensed Matter–2005*** (Furnish MD, Elert M, Russell TP, and White CT, Eds.) AIP Conf. Series 845, 1391-1394, AIP, Melville, NY (2006).

4. Orphal DL, Anderson CE Jr., Behner T, Hohler V, Wickert M, and Templeton DW. Failure kinetics in borosilicate glass during rod impact. ***Shock Compression of Condensed Matter—2007*** (Elert M, *et al.*, Eds.) AIP Conf. Series 955, pp. 759-762, AIP, Melville, NY (2007).

5. Orphal DL. Some recent results on the propagation of the failure front associated with rod penetration of borosilicate glass. ***Shock Compression in Condensed Matter****—2009* (Elert M, *et. al.*, Eds.), Conf. Proc., AIP, Melville, NY, in press (2009).

6. Behner T, Anderson CE Jr., Orphal DL, Hohler V, Moll M, and Templeton DW. Penetration and failure of lead and borosilicate glass against rod Impact. *Int. J. Impact Engng.*, **35**(6): 447-456, (2008).

7. Anderson CE Jr., Orphal DL, Behner T, and Templeton DW. Failure and penetration response of borosilicate glass during short-rod impact. *Int. J. Impact Engng.*, **36**(6): 789-798 (2009).

8. Orphal DL, Anderson CE Jr., Behner T, and Templeton DW. Failure and penetration response of borosilicate glass during multiple short-rod impact. *Int. J. Impact Engng.*, **36**(10-11): 1173-1181 (2009).

9. Anderson CE Jr., Behner T, Orphal DL, Holmquist TJ, Hohler V, and Wickert M. Interface defeat of long rods impacting borosilicate glass experimental results. SwRI Report 18.12544/009, prepared for RDECOM-TARDEC, AMSRD-TAR-R, Warren, MI, February (2009).

10. Anderson CE Jr., Holmquist TJ, Orphal DL, and Behner T. Dwell and interface defeat on glass targets. *Int. J. Appl. Ceram. Technol.*, submitted.

11. Strassburger E and Senf H. Experimental investigations of wave and fracture phenomena in impacted ceramics and glasses. Report ARL-CR-214, Army Research Laboratory, Aberdeen Proving Ground, MD (1995).

12. Strassburger E, Patel P, McCauley JW, and Templeton DW. High-speed photographic study of wave and fracture propagation in fused silica. *Proc. 22nd Int. Symp. Ballistics*, 2: 761-768, DES*tech* Publications, Inc., Lancaster, PA (2005).

13. Grady DE. Presentation at TARDEC Glass Workshop, Detroit, MI, 7-8 May (2008).

14. Tuler FR and Butcher BM. A criterion for the time dependency of dynamic fracture. *Int. J. Fract. Mech.*, **4**(4): 431-437 (1968).

15. Anderson CE Jr., Mullin SA and Kuhlman CJ. Computer simulation of strain-rate effects in replica scale model penetration experiments. *Int. J. Impact Engng*., **13**(1): 35-52 (1993).

16. Anderson CE Jr., Mullin SA, Piekutowski AJ, Blaylock NW, and Poormon KL. Scale model experiments with ceramic laminate targets. *Int. J. Impact Engng.*, **18**(1): 1-22 (1996).

17. Wereszczak AA, Kirtland, TP, Ragan, ME, Strong KT Jr., and Patel, P. Size-scaling of tensile failure stress in a float soda-lime silicate glass. *Int. J. Appl. Glass Sci.*, to be submitted (2009).

18. Chocron S, Dannemann KA, Nicholls AE, and Anderson CE Jr. Characterization of borosilicate glass by confined compression testing and numerical validation. SwRI Report 18.12544/010, prepared for RDECOM-TARDEC, AMSRD-TAR-R, Warren, MI (2009).

19. Curran DR, Seaman L, and Shockey DA. Dynamic failure of solids. *Physics Reports (Review Section of Physics Letters)*, **145**(5&6): 253-388 (1987).

20. Alexander CS, Chhabildas LC, Reinhart WD, and Templeton DW. Changes to the shock response of fused quartz due to glass modification. *Int. J. Impact Engng.*, **35**(12): 1376-1385 (2008).

21. Johnson GR and Holmquit TJ. Test data and computational strength and fracture model constants for 23 materials subjected to large strains, high strain rates and temperatures. LA-11463-MS, Los Alamos National Laboratory, Los Alamos, NM (1989).

22. Johnson GR and Cook WH. A constitutive model and data for metals subjected to large strains, high strain rates and high temperatures. *Proc. 7th Int. Symp. Ballistics*, pp. 541-548, he Hague, The Netherlands (1983).

23. Johnson GR and Cook WH. Fracture characteristics of three metals subjected to various strains, strain rates, temperatures and pressures. *Engng. Fract. Mech.*, **21**(1): 31-48 (1985).

24. Zukas JA. Penetration and perforation of solids. Chapter 5 in ***Impact Dynamics*** (Zukas JA, Nicholas T, Swift HF, Greszczuk LB, and Curran DR), John Wiley & Sons, NY, NY (1982).

25. Orphal DL. Private communication (2009).

26. Anderson CE Jr. and Walker JD. An analytical model for dwell and interface defeat. *Int. J. Impact Engng.*, **31**(9): 1119-1132 (2005).

27. Anderson CE Jr. Presentation at TARDEC Glass Workshop, Menlo Park, CA, 5-6 September (2007).

28. Anderson CE Jr., Behner T, Holmquist TJ, Orphal DL, and Wickert M. Dwell, interface defeat, and penetration of long rods impacting silicon carbide. SwRI Report 18.12544/008, prepared for RDECOM-TARDEC, AMSRD-TAR-R, Warren, MI, April (2009).

APPENDIX A: TABULATED DATA

Table A1. Lexan Target: 0.22-cal Bullet

Test #	Target	V_s (m/s)	V_r (m/s)	W_o (g)	L_o (cm)	W_r (g)	L_r (cm)	Pass/Fail
99	0.22-in Lexan	978	937	2.320	1.671	2.318	1.674	CP
100	0.22-in Lexan	863	817	2.316	1.669	2.302	1.575	CP
101	0.22-in Lexan	776	721	2.316	1.669	2.310	1.646	CP
102	0.22-in Lexan	607	562	2.314	1.674	2.316	1.676	CP
103	0.22-in Lexan	560	508	2.322	1.669	2.320	1.674	CP
104	0.22-in Lexan	482	418	2.324	1.674	2.320	1.674	CP
106	0.22-in Lexan	489	424	2.324	1.669	2.322	1.676	CP
105	0.22-in Lexan	463	414	2.324	1.669	2.324	1.674	CP
106	0.22-in Lexan	463	414	2.324	1.669	2.322	1.674	CP
107	0.22-in Lexan	349	283	2.322	1.674	2.320	1.676	CP
108	0.22-in Lexan	307	231	2.322	1.671	2.320	1.674	CP
109	0.22-in Lexan	304	233	2.324	1.669	2.320	1.676	CP
	Average			2.321	1.670	2.318	1.664	
	Standard Deviation			0.004	0.002	0.006	0.029	

Table A2. Lexan Target: 0.375-cal Bullet

Test #	Target	V_s (m/s)	V_r (m/s)	W_o (g)	L_o (cm)	W_r (g)	L_r (cm)	Pass/Fail
111	.375-in Lexan	365	287	11.512	2.845	unk	unk	CP
112	.375-in Lexan	254	176	11.542	2.845	unk	unk	CP
113	.375-in Lexan	195	60	11.544	2.865	11.484	2.858	CP
114	.375-in Lexan	133	0	11.504	2.845	11.504	2.852	PP
115	.375-in Lexan	163	0	11.532	2.845	11.530	2.855	PP
116	.375-in Lexan	211	104	11.396	2.817	11.394	2.822	CP
117	.375-in Lexan	486	439	11.530	2.842	11.528	2.855	CP
118	.375-in Lexan	545	496	11.506	2.830	11.148	2.639	CP
119	.375-in Lexan	643	598	11.518	2.845	11.500	2.835	CP
120	.375-in Lexan	890	852	11.646	2.858	11.516	2.850	CP
121	.375-in Lexan	782	735	11.544	2.858	9.352	2.060	CP
122	.375-in Lexan	380	314	11.534	2.858	11.530	2.870	CP
	Average			11.526	2.846	11.249	2.750	
	Standard Deviation			0.055	0.013	0.677	0.252	

Table A3. Lexan Target: 0.50-cal Bullet

Test #	Target	V_s (m/s)	V_r (m/s)	W_o (g)	L_o (cm)	W_r (g)	L_r (cm)	Pass/Fail
123	0.50-in Lexan	215	unk	27.766	3.800	27.766	3.810	CP
124	0.50-in Lexan	148	0	27.546	3.795	27.546	3.807	PP
125	0.50-in Lexan	214	128	27.672	3.795	27.670	3.805	CP
126	0.50-in Lexan	181	54	27.720	3.797	27.720	3.807	CP
127	0.50-in Lexan	164	0	27.664	3.795	27.660	3.807	PP
128	0.50-in Lexan	186	69	27.538	3.792	27.536	4.051	CP
129	0.50-in Lexan	555	515	27.548	3.795	27.534	3.807	CP
130	0.50-in Lexan	499	454	27.522	3.792	27.512	3.805	CP
131	0.50-in Lexan	423	387	27.716	3.800	27.712	3.810	CP
132	0.50-in Lexan	342	298	27.570	3.797	27.566	3.807	CP
133	0.50-in Lexan	255	188	27.870	3.795	27.870	3.802	CP
134	0.50-in Lexan	740	717	27.520	3.799	27.500	3.807	CP
201	0.50-in Lexan	820	784	27.600	3.800	27.580	3.787	CP
202	0.50-in Lexan	897	864	27.510	3.796	27.460	3.790	CP
203	0.50-in Lexan	278	207	27.570	3.790	unk	unk	CP
204	0.50-in Lexan	619	598	27.580	3.791	unk	unk	CP
	Average			27.626	3.796	27.617	3.822	
	Standard Deviation			0.111	0.003	0.118	0.066	

Table A4. Monoblock Glass Target: 0.22-cal Bullet

Test #	Threat	Target	V_s (m/s)	V_r (m/s)	W_o (g)	L_o (cm)	W_r (g)	L_r (cm)	Pass/Fail	W_r/W_s	L_r/L_s
63	.22cal	9.24mm BF	497	223	2.324	1.668	1.872	1.115	CP	0.806	0.669
64	.22cal	9.24mm BF	404	144	2.324	1.668	unk	1.131	CP	–	0.678
65	.22cal	9.24mm BF	647	307	2.320	1.668	2.002	1.331	CP	0.863	0.798
66	.22cal	9.24mm BF	751	511	2.322	1.665	2.234	1.361	CP	0.962	0.818
67	.22cal	9.24mm BF	925	759	2.324	1.666	2.240	1.590	CP	0.964	0.954
68	.22cal	9.24mm BF	592	305	2.328	1.669	2.148	1.207	CP	0.923	0.723
69	.22cal	9.24mm BF	342	100	2.330	1.668	2.142	1.306	CP	0.919	0.783
70	.22cal	9.24mm BF	305	116	2.328	1.665	unk	1.410	CP	–	0.847
71	.22cal	9.24mm BF	318	88	2.328	1.664	2.162	1.311	CP	0.929	0.788
72	.22cal	9.24mm BF	267	unk	2.326	1.664	2.178	1.381	CP	0.936	0.820
73	.22cal	9.24mm BF	271	94	2.326	1.664	2.214	1.352	CP	0.952	0.812

Table A5. Monoblock Glass Target: 0.375-cal Bullet

Test #	Threat	Target	V_s (m/s)	V_r (m/s)	W_o (g)	L_o (cm)	W_r (g)	L_r (cm)	Pass/Fail	W_r/W_s	L_r/L_s
32	.375cal	15.75mm BF	546	286	11.50	2.847	9.20	1.933	CP	0.800	0.678
33	.375cal	15.75mm BF	479	211	11.50	2.845	9.87	2.073	CP	0.858	0.732
34	.375cal	15.75mm BF	441	226	11.45	2.842	10.08	2.162	CP	–	0.715
35	.375cal	15.75mm BF	397	178	11.45	2.845	10.56	2.189	CP	0.922	0.777
36	.375cal	15.75mm BF	366	197	11.45	2.845	10.92	2.337	CP	0.954	0.821
37	.375cal	15.75mm BF	291	137	11.55	2.845	11.19	2.390	CP	0.969	0.839
38	.375cal	15.75mm BF	242	72	11.51	2.842	11.15	2.393	CP	0.969	0.849
39	.375cal	15.75mm BF	273	128	11.52	2.845	11.08	2.316	CP	0.962	0.813
40	.375cal	15.75mm BF	662	unk	11.53	2.845	10.74	2.184	CP	0.931	0.768
41	.375cal	15.75mm BF	667	501	11.51	2.842	11.25	2.428	CP	0.977	0.858
42	.375cal	15.75mm BF	798	656	11.5	2.837	unk	2.134	CP	–	0.922
43	.375cal	15.75mm BF	939	812	11.51	2.845	unk	2.718	CP	–	0.955
44	.375cal	15.75mm BF	282	91	11.51	2.845	10.78	2.283	CP	0.937	0.804
45	.375cal	15.75mm BF	195	46	11.51	2.847	unk	2.286	CP	–	0.803
46	.375cal	15.75mm BF	216	73	11.53	2.847	11.20	2.383	CP	0.971	0.839

Table A6. Monoblock Glass Target: 0.50-cal Bullet

Test #	Threat	Target	V_s (m/s)	V_r (m/s)	W_o (g)	L_o (cm)	W_r (g)	L_r (cm)	Pass/Fail	W_r/W_s	L_r/L_s
5	.50cal	21mm BF	257	unk	27.90	3.790	26.86	3.145	CP	0.963	0.830
6	.50cal	21mm BF	233	101	27.50	3.790	26.89	3.208	CP	0.978	0.847
7	.50cal	21mm BF	187	70	27.50	3.795	26.96	3.246	CP	0.980	0.855
8	.50cal	21mm BF	161	46	27.50	3.795	27.04	3.366	CP	0.983	0.887
9	.50cal	21mm BF	187	71	27.50	3.797	27.08	3.274	CP	0.985	0.862
10	.50cal	21mm BF	309	151	27.50	3.790	26.64	3.178	CP	0.969	0.838
11	.50cal	21mm BF	371	191	27.50	3.795	26.74	3.114	CP	0.972	0.821
12	.50cal	21mm BF	402	237	27.50	3.795	26.15	3.051	CP	0.951	0.804
13*	.50cal	21mm BF	442	202	27.50	3.795	23.50	2.898	CP	0.855	0.764
14	.50cal	21mm BF	443	265	27.50	3.797	25.70	2.944	CP	0.935	0.775
15	.50cal	21mm BF	483	271	27.60	3.795	25.00	2.987	CP	0.906	0.787
16	.50cal	21mm BF	543	307	27.60	3.797	25.40	3.101	CP	0.920	0.817
17	.50cal	21mm BF	620	463	27.50	3.787	27.10	3.599	CP	0.985	0.950
172	.50cal	21mm BF	626	430	27.52	3.796	26.32	3.175	CP	0.956	0.836
173	.50cal	21mm BF	735	602	27.57	3.791	27.45	3.668	CP	0.996	0.968
174	.50cal	21mm BF	821	696	27.55	3.793	27.38	3.586	CP	0.994	0.945
175	.50cal	21mm BF	898	755	27.55	3.795	27.42	3.698	CP	0.995	0.975

Table A7. Bonded Glass Target: 0.22-cal Bullet

Test #	Threat	Target	V_s (m/s)	V_r (m/s)	W_o (g)	L_o (cm)	W_r (g)	L_r (cm)	Pass/Fail	W_r/W_s	L_r/L_s
49	.22cal	9.24mm BF w/ Lex	748	unk	2.322	1.669	2.250	1.382	CP	0.969	0.828
50	.22cal	9.24mm BF w/ Lex	745	unk	2.326	1.669	2.250	1.405	CP	0.967	0.839
51	.22cal	9.24mm BF w/ Lex	745	375	2.322	1.669	2.260	1.415	CP	0.973	0.848
52	.22cal	9.24mm BF w/ Lex	583	0	2.318	1.669	1.744	1.161	PP	0.752	0.696
53	.22cal	9.24mm BF w/ Lex	688	302	2.32	1.669	2.214	1.521	CP	0.954	0.840
54	.22cal	9.24mm BF w/ Lex	750	433	2.32	1.664	unk	1.242	CP	–	0.747
55	.22cal	9.24mm BF w/ Lex	966	700	2.326	1.669	unk	1.590	CP	–	0.953
56	.22cal	9.24mm BF w/ Lex	866	609	2.326	1.669	2.300	1.557	CP	0.989	0.933
57	.22cal	9.24mm BF w/ Lex	815	543	2.316	1.669	2.286	1.524	CP	0.987	0.909
58	.22cal	9.24mm BF w/ Lex	566	0	2.326	1.669	unk	unk	PP	–	–
59	.22cal	9.24mm BF w/ Lex	663	190	2.322	1.669	2.020	1.427	CP	0.870	0.855
60	.22cal	9.24mm BF w/ Lex	618	196	2.324	1.664	unk	1.316	CP	–	0.791
61	.22cal	9.24mm BF w/ Lex	595	0	2.322	1.669	2.042	1.461	PP	0.879	0.871
62	.22cal	9.24mm BF w/ Lex	625	91	2.322	1.669	1.894	1.275	CP	0.816	0.760

Table A8. Bonded Glass Target: 0.375-cal Bullet

Test #	Threat	Target	V_s (m/s)	V_r (m/s)	W_o (g)	L_o (cm)	W_r (g)	L_r (cm)	Pass/Fail	W_r/W_s	L_r/L_s
21	.375cal	15.75mm BF w/Lex	645	301	11.51	2.845	unk	2.057	CP	–	0.723
22	.375cal	15.75mm BF w/Lex	549	0	11.50	2.845	9.50	2.278	PP	0.826	0.801
23	.375cal	15.75mm BF w/Lex	578	0	11.52	2.847	9.40	2.286	PP	0.816	0.803
24	.375cal	15.75mm BF w/Lex	619	0	11.52	2.842	8.70	2.080	PP	0.755	0.732
25	.375cal	15.75mm BF w/Lex	627	0	11.54	2.842	8.60	2.062	PP	0.745	0.726
26	.375cal	15.75mm BF w/Lex	664	unk	11.55	2.842	10.80	2.319	CP	0.935	0.816
27	.375cal	15.75mm BF w/Lex	724	392	11.45	2.845	10.50	2.261	CP	0.917	0.795
28	.375cal	15.75mm BF w/Lex	803	580	11.50	2.842	unk	2.616	CP	–	0.920
29	.375cal	15.75mm BF w/Lex	799	562	11.45	2.842	unk	2.362	CP	–	0.831
30	.375cal	15.75mm BF w/Lex	864	647	11.45	2.842	unk	2.616	CP	–	0.920
31	.375cal	15.75mm BF w/Lex	934	724	11.45	2.845	unk	2.616	CP	–	0.920
47	.375cal	15.75mm BF w/Lex	645	unk	11.53	2.845	11.12	2.456	CP	0.964	0.863
48	.375cal	15.75mm BF w/Lex	614	0	11.48	2.835	10.38	2.182	PP	0.904	0.770

Table A9. Bonded Glass Target: 0.50-cal Bullet

Test #	Threat	Target	V_s (m/s)	V_r (m/s)	W_o (g)	L_o (cm)	W_r (g)	L_r (cm)	Pass/Fail	W_r/W_s	L_r/L_s
18	.50cal	21mm BF w/ Lex	307	0	27.6	3.795	26.200	3.040	PP	0.949	0.801
19	.50cal	21mm BF w/ Lex	516	0	27.5	3.800	18.500	2.174	PP	0.673	0.572
20	.50cal	21mm BF w/ Lex	571	0	27.5	3.792	23.600	2.819	PP	0.858	0.740
165	.50cal	21mm BF w/ Lex	911	704	27.49	3.797	26.950	3.627	CP	0.980	0.955
166	.50cal	21mm BF w/ Lex	740	531	27.57	3.793	27.300	3.683	CP	0.990	0.971
167	.50cal	21mm BF w/ Lex	603	0	27.56	3.795	unk	2.497	PP	–	0.658
168	.50cal	21mm BF w/ Lex	657	446	27.54	3.792	27.400	3.724	CP	0.995	0.983
169	.50cal	21mm BF w/ Lex	627	275	27.55	3.786	26.390	3.150	CP	0.958	0.832
170	.50cal	21mm BF w/ Lex	591	0	27.53	3.800	23.610	3.020	PP	0.858	0.795
171	.50cal	21mm BF w/ Lex	636	242	27.55	3.795	26.390	3.099	CP	0.958	0.813

Table A10. Multi-Hit Bonded Glass Target: 0.22-cal Bullet

Test #	Test Seq.	Threat	Target	V_s (m/s)	V_r (m/s)	W_o (g)	L_o (cm)	W_r (g)	L_r (cm)	Pass/Fail	W_r/W_s	L_r/L_s
74	1	.22cal	9.24mm BF w/ Lex	625	0	2.320	1.664	1.636	1.011	PP	0.705	0.608
75	2	.22cal	9.24mm BF w/ Lex	610	381	2.320	1.666	2.254	1.405	CP	0.972	0.843
76	3	.22cal	9.24mm BF w/ Lex	644	428	2.320	1.666	2.300	1.567	CP	0.991	0.941
77	4	.22cal	9.24mm BF w/ Lex	447	171	2.320	1.664	2.250	1.392	CP	0.970	0.837
78	5	.22cal	9.24mm BF w/ Lex	371	unk	2.320	1.664	2.316	1.641	CP	0.998	0.986
79	1	.22cal	9.24mm BF w/ Lex	753	371	2.322	1.666	2.226	1.499	CP	0.959	0.899
80	2	.22cal	9.24mm BF w/ Lex	747	484	2.318	1.661	2.284	1.577	CP	0.985	0.950
81	3	.22cal	9.24mm BF w/ Lex	752	511	2.320	1.664	2.306	1.621	CP	0.994	0.974
82	4	.22cal	9.24mm BF w/ Lex	382	0	2.318	1.664	2.316	1.588	PP	0.999	0.954
83	5	.22cal	9.24mm BF w/ Lex	426	0	2.320	1.664	2.294	1.458	PP	0.989	0.876
84	1	.22cal	9.24mm BF w/ Lex	851	595	2.322	1.664	2.314	1.636	CP	0.997	0.983
85	2	.22cal	9.24mm BF w/ Lex	851	604	2.320	1.661	2.290	1.483	CP	0.987	0.893
86	3	.22cal	9.24mm BF w/ Lex	847	609	2.324	1.664	unk	unk	CP	–	–
87	4	.22cal	9.24mm BF w/ Lex	503	214	2.322	1.664	2.152	1.273	CP	0.927	0.765
88	5	.22cal	9.24mm BF w/ Lex	437	0	2.326	1.664	2.166	1.420	PP	0.931	0.853
89	1	.22cal	9.24mm BF w/ Lex	603	77	2.322	1.669	1.864	1.227	CP	0.803	0.735
90	2	.22cal	9.24mm BF w/ Lex	575	264	2.324	1.671	2.306	1.641	CP	0.992	0.982

Test #	Test Seq.	Threat	Target	V_s (m/s)	V_r (m/s)	W_o (g)	L_o (cm)	W_r (g)	L_r (cm)	Pass/Fail	W_r/W_s	L_r/L_s
91	3	.22cal	9.24mm BF w/ Lex	580	260	2.324	1.669	2.304	1.575	CP	0.991	0.944
92	4	.22cal	9.24mm BF w/ Lex	461	71	2.330	1.669	1.868	1.280	CP	0.802	0.767
93	5	.22cal	9.24mm BF w/ Lex	unk	135	2.328	1.671	2.300	1.496	CP	–	–
94	1	.22cal	9.24mm BF w/ Lex	983	703	2.322	1.674	unk	unk	CP	–	–
95	2	.22cal	9.24mm BF w/ Lex	974	759	2.322	1.669	2.290	1.461	CP	0.986	0.875
96	3	.22cal	9.24mm BF w/ Lex	975	755	2.324	1.666	1.948	1.588	CP	0.838	0.953
97	4	.22cal	9.24mm BF w/ Lex	337	0	2.326	1.671	2.114	1.306	PP	0.909	0.781
98	5	.22cal	9.24mm BF w/ Lex	419	0	2.328	1.671	2.288	1.491	PP	0.983	0.892

Table A11. Multi-Hit Bonded Glass Target: 0.375-cal Bullet

Test #	Test Seq.	Threat	Target	V_s (m/s)	V_r (m/s)	W_o (g)	L_o (cm)	W_r (g)	L_r (cm)	Pass/Fail	W_r/W_s	L_r/L_s
135	1	.357cal	15.75mm BF w/Lex	874	651	11.54	2.870	11.51	2.852	CP	0.998	0.994
136	2	.357cal	15.75mm BF w/Lex	873	667	11.54	2.858	11.48	2.845	CP	0.995	0.996
137	3	.357cal	15.75mm BF w/Lex	885	717	11.52	2.852	11.43	2.822	CP	0.993	0.989
138	4	.357cal	15.75mm BF w/Lex	skipped	—	—	—	—	—	—	—	—
139	5	.357cal	15.75mm BF w/Lex	skipped	—	—	—	—	—	—	—	—
140	1	.357cal	15.75mm BF w/Lex	818	611	11.56	2.852	8.74	2.718	CP	0.756	0.953
141	2	.357cal	15.75mm BF w/Lex	819	611	11.54	2.858	11.43	2.705	CP	0.991	0.947
142	3	.357cal	15.75mm BF w/Lex	823	643	11.54	2.852	unk	unk	CP	unk	unk
143	4	.357cal	15.75mm BF w/Lex	skipped	—	—	—	—	—	—	—	—
144	5	.357cal	15.75mm BF w/Lex	skipped	—	—	—	—	—	—	—	—
145	1	.357cal	15.75mm BF w/Lex	715	512	11.56	2.858	11.34	2.464	CP	0.981	0.862
146	2	.357cal	15.75mm BF w/Lex	718	498	11.54	2.858	11.43	2.779	CP	0.990	0.972
147	3	.357cal	15.75mm BF w/Lex	714	541	11.54	2.858	unk	unk	CP	unk	unk
148	4	.357cal	15.75mm BF w/Lex	539	390	11.55	2.858	11.49	2.725	CP	0.995	0.954
149	5	.357cal	15.75mm BF w/Lex	415	0	11.55	2.858	11.11	2.464	PP	0.962	0.862
150	1	.357cal	15.75mm BF w/Lex	602	0	11.53	2.858	10.20	2.311	PP	0.885	0.809

Test #	Test Seq.	Threat	Target	V_s (m/s)	V_r (m/s)	W_o (g)	L_o (cm)	W_r (g)	L_r (cm)	Pass/Fail	W_r/W_s	L_r/L_s
151	2	.357cal	15.75mm BF w/Lex	610	390	11.56	2.855	11.31	2.522	CP	0.979	0.883
152	3	.357cal	15.75mm BF w/Lex	620	432	11.55	2.858	11.48	2.629	CP	0.994	0.920
153	4	.357cal	15.75mm BF w/Lex	468	288	11.55	2.858	11.32	2.456	CP	0.980	0.860
154	5	.357cal	15.75mm BF w/Lex	404	213	11.58	2.860	11.47	2.677	CP	0.991	0.936
155	1	.357cal	15.75mm BF w/Lex	813	582	11.55	2.858	11.47	2.797	CP	0.993	0.979
156	2	.357cal	15.75mm BF w/Lex	790	612	11.56	2.858	8.30	2.718	CP	0.996	0.951
157	3	.357cal	15.75mm BF w/Lex	786	611	11.54	2.852	unk	unk	CP	unk	unk
158	4	.357cal	15.75mm BF w/Lex	369	123	11.56	2.858	11.51	2.723	CP	0.996	0.953
159	5	.357cal	15.75mm BF w/Lex	339	136	11.54	2.855	unk	unk	CP	unk	unk
160	1	.357cal	15.75mm BF w/Lex	660	0	11.54	2.858	9.72	2.169	PP	0.842	0.759
161	2	.357cal	15.75mm BF w/Lex	661	494	11.52	2.855	11.47	2.812	CP	0.996	0.985
162	3	.357cal	15.75mm BF w/Lex	633	434	11.55	2.858	unk	unk	CP	unk	unk
163	4	.357cal	15.75mm BF w/Lex	493	282	11.55	2.858	11.39	2.512	CP	0.986	0.879
164	5	.357cal	15.75mm BF w/Lex	233	0	11.55	2.858	11.54	2.786	PP	0.999	0.975
205	1	.375cal	15.75mm BF w/Lex	675	0	not measured				PP	not measured	
206	2	.375cal	15.75mm BF w/Lex	386	52	not measured				CP	not measured	
207	3	.375cal	15.75mm BF w/Lex	446	227	not measured				CP	not measured	

Test #	Test Seq.	Threat	Target	V_s (m/s)	V_r (m/s)	W_o (g)	L_o (cm)	W_r (g)	L_r (cm)	Pass/Fail	W_r/W_s	L_r/L_s
208	4	.375cal	15.75mm BF w/Lex	353	0		not measured			PP	not measured	
209	5	.375cal	15.75mm BF w/Lex	479	315		not measured			CP	not measured	

Table A12. Multi-Hit Bonded Glass Target: 0.50-cal Bullet

Test #	Test Seq.	Threat	Target	V_s (m/s)	V_r (m/s)	W_o (g)	L_o (cm)	W_r (g)	L_r (cm)	Pass/Fail	W_r/W_s	L_r/L_s
176	1	.50cal	21mm BF w/ Lex	911	688	27.50	3.787	unk	unk	CP	–	–
177	2	.50cal	21mm BF w/ Lex	903	718	27.60	3.799	27.43	3.665	CP	0.994	0.965
178	3	.50cal	21mm BF w/ Lex	900	716	27.49	3.793	27.31	3.724	CP	0.993	0.982
179	4	.50cal	21mm BF w/ Lex	632	491	27.56	3.796	27.46	3.665	CP	0.996	0.966
180	5	.50cal	21mm BF w/ Lex	488	344	27.44	3.786	27.37	3.668	CP	0.997	0.969
181	1	.50cal	21mm BF w/ Lex	814	610	27.59	3.796	unk	unk	CP	–	–
182	2	.50cal	21mm BF w/ Lex	815	645	27.50	3.796	27.33	3.603	CP	0.994	0.949
183	3	.50cal	21mm BF w/ Lex	825	677	27.57	3.795	27.20	3.658	CP	0.987	0.964
184	4	.50cal	21mm BF w/ Lex	499	286	27.52	3.793	27.40	3.640	CP	0.996	0.959
185	5	.50cal	21mm BF w/ Lex	436	298	27.57	3.795	27.51	3.656	CP	0.998	0.964
186	1	.50cal	21mm BF w/ Lex	730	496	27.52	3.802	27.27	3.556	CP	0.991	0.935
187	2	.50cal	21mm BF w/ Lex	731	568	27.52	3.799	unk	unk	CP	–	–
188	3	.50cal	21mm BF w/ Lex	730	569	27.54	3.796	unk	unk	CP	–	–
189	4	.50cal	21mm BF w/ Lex	387	unk	27.50	3.790	27.16	3.344	CP	0.988	0.882
190	5	.50cal	21mm BF w/ Lex	426	280	27.55	3.795	27.51	3.741	CP	0.999	0.986
191	1	.50cal	21mm BF w/ Lex	613	229	27.46	3.792	26.38	3.113	CP	0.961	0.821

Test #	Test Seq.	Threat	Target	V_s (m/s)	V_r (m/s)	W_o (g)	L_o (cm)	W_r (g)	L_r (cm)	Pass/Fail	W_r/W_s	L_r/L_s
192	2	.50cal	21mm BF w/ Lex	628	443	27.59	3.792	27.42	3.526	CP	0.994	0.930
193	3	.50cal	21mm BF w/ Lex	625	436	27.50	3.793	27.35	3.609	CP	0.995	0.951
194	4	.50cal	21mm BF w/ Lex	343	88	27.45	3.793	27.27	3.480	CP	0.993	0.917
195	5	.50cal	21mm BF w/ Lex	272	0	27.51	3.791	27.48	3.701	PP	0.999	0.976
196	1	.50cal	21mm BF w/ Lex	553	0	27.54	3.795	21.96	2.606	PP	0.797	0.687
197	2	.50cal	21mm BF w/ Lex	541	362	27.54	3.792	27.41	3.585	CP	0.995	0.945
198	3	.50cal	21mm BF w/ Lex	553	394	27.57	3.793	27.35	3.452	CP	0.992	0.910
199	4	.50cal	21mm BF w/ Lex	305	0	27.48	3.796	27.42	3.632	PP	0.998	0.957
200	5	.50cal	21mm BF w/ Lex	311	0	27.46	3.791	27.24	3.494	PP	0.992	0.922